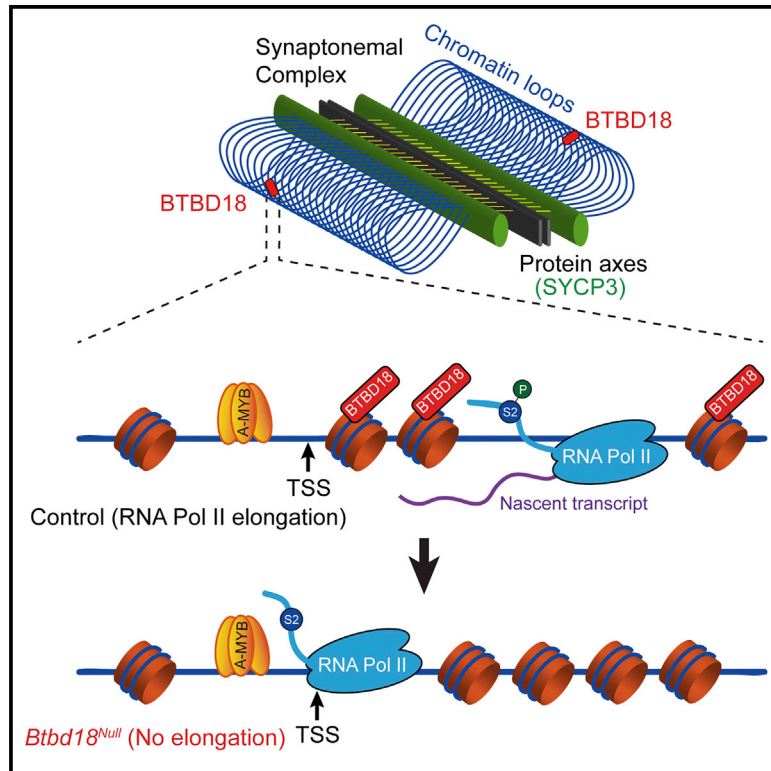


Developmental Cell

BTBD18 Regulates a Subset of piRNA-Generating Loci through Transcription Elongation in Mice

Graphical Abstract



Authors

Liquan Zhou, Bertram Canagarajah, Yangu Zhao, Boris Baibakov, Keizo Tokuhira, Dragan Maric, Jurrien Dean

Correspondence

li-quan.zhou@nih.gov (L.Z.), jurrien.dean@nih.gov (J.D.)

In Brief

piRNAs are small non-coding RNAs primarily expressed in animal gonads. Zhou et al. implicate BTBD18, a nuclear protein, in piRNA biogenesis as key for male fertility. BTBD18 binds to a subset of pachytene piRNA-producing loci in mouse testes, promotes transcription elongation, and promotes piRNA precursor expression for successful germ cell development.

Highlights

- Present in pachytene nuclei, BTBD18 is essential for spermiogenesis in mice
- BTBD18 occupies a subset of pachytene piRNA loci with genome-wide specificity
- Pachytene piRNA loci are regulated by BTBD18-dependent transcription elongation
- Different chromatin structures correlate with BTBD18 occupancy



BTBD18 Regulates a Subset of piRNA-Generating Loci through Transcription Elongation in Mice

Liquan Zhou,^{1,*} Bertram Canagarajah,¹ Yangu Zhao,¹ Boris Baibakov,¹ Keizo Tokuhiro,¹ Dragan Maric,² and Jurrien Dean^{1,3,*}

¹Laboratory of Cellular and Developmental Biology, NIDDK

²NINDS Flow Cytometry Core Facility

National Institutes of Health, Bethesda, MD 20892, USA

³Lead Contact

*Correspondence: li-quan.zhou@nih.gov (L.Z.), jurrien.dean@nih.gov (J.D.)

<http://dx.doi.org/10.1016/j.devcel.2017.02.007>

SUMMARY

PIWI-interacting RNAs (piRNAs) are small non-coding RNAs essential for animal germ cell development. Despite intense investigation of post-transcriptional processing, chromatin regulators for piRNA biogenesis in mammals remain largely unexplored. Here we document that BTBD18 is a pachytene nuclear protein in mouse testes that occupies a subset of pachytene piRNA-producing loci. Ablation of *Btbd18* in mice disrupts piRNA biogenesis, prevents spermiogenesis, and results in male sterility. Transcriptome profiling, chromatin accessibility, and RNA polymerase II occupancy demonstrate that BTBD18 facilitates expression of pachytene piRNA precursors by promoting transcription elongation. Thus, our study identifies BTBD18 as a specific controller for transcription activation through RNA polymerase II elongation at a subset of genomic piRNA loci.

INTRODUCTION

PIWI-interacting RNAs (piRNAs) are the largest class of small non-coding RNAs in animals. They are primarily expressed in gonads in both vertebrates and invertebrates, including worms, flies, and mammals, with partially conserved features. They are 26- to 31-nt silencing RNAs derived from single-stranded RNA precursors, modified at 3' termini by 2'-O-methylation, and processed by PIWI-clade Argonaute proteins. In mammals, piRNAs are highly abundant in testis, the male gonad for spermatogenesis. Mutation of piRNA pathway genes in mice, including those encoding PIWI family and accessory proteins, leads to male sterility (Aravin and Hannon, 2008; Deng and Lin, 2002).

The most well-studied piRNA population originates from clusters of genomic transposons and is amplified by the ping-pong cycle. These piRNAs are expressed in fly gonads, prenatal murine testes (fetal piRNAs), and early postnatal murine testes (pre-pachytene piRNAs). They silence transposable elements and maintain genome integrity during gametogenesis. Disruption of piRNA pathways in mice leads to unsuppressed retrotransposon expression (Saxe et al., 2013; De Fazio et al., 2011;

Reuter et al., 2011; Soper et al., 2008). Deep sequencing of small RNAs documents that piRNAs are also processed from mRNAs in fly ovaries and postnatal murine testes, especially from 3' UTRs, for an as yet unclear function (Robine et al., 2009). However, the most highly enriched piRNAs in adult murine testes are termed pachytene piRNAs because of their accumulation beginning in the pachytene phase of meiotic prophase I. These piRNAs exist in mice but not flies, and originate primarily from non-transposon, intergenic, long non-coding RNAs that map uniquely in the genome. Pachytene piRNA biogenesis does not involve ping-pong amplification, introduction of which leads to secondary piRNA generation and male sterility in mice (Wasik et al., 2015). Accumulating evidence indicates that pachytene piRNAs may progressively eliminate mRNAs and long non-coding RNAs during spermatogenesis to support successful germline development (Goh et al., 2015; Gou et al., 2015; Watanabe et al., 2015; Yamamoto et al., 2013), although the mechanism by which pachytene piRNAs target non-repeat mRNA sequences is not fully understood (Vourekas et al., 2012).

Despite extreme complexity (i.e., hundreds of thousands of different piRNA species in mammals), pachytene piRNA sequences originate from only a few hundred discrete genomic loci (Aravin et al., 2006; Girard et al., 2006; Lau et al., 2006) and are strongly selected for germline development. Introduction of one human pachytene piRNA cluster into the mouse genome reshaped the piRNA transcriptome and caused male sterility (Goh et al., 2015). Generally, pachytene piRNAs either distribute across one genomic strand or distribute divergently without overlap. These long primary transcripts are driven by RNA polymerase II (Pol II) and have both 5' caps and 3' poly(A) tails (Li et al., 2013). Random insertion of a modified pachytene piRNA cluster into non-native genomic positions in mice produces functional artificial piRNA populations, indicating that regulatory signals for piRNA precursor activation lie within the loci (Muerdter et al., 2012). Detailed mechanisms of transcriptional regulation of pachytene piRNAs are poorly understood. The only transcription regulator identified so far is A-MYB (encoded by *Myb17*), a master regulator of male meiosis (Bolcun-Filas et al., 2011). A-MYB is an ancient transcription factor expressed in both mice and flies. It is essential for activation of pachytene piRNA precursors as well as multiple meiotic genes, with its binding sites proximal to their transcription start sites (Li et al., 2013).

The BTB domain is known as a protein-protein interaction motif at the N terminus of multiple factors regulating a variety

of biological events including transcription, protein degradation, and tumorigenesis (Perez-Torrado et al., 2006). Here, we assess the role of BTBD18, a previously uncharacterized BTB-domain-containing protein, during mouse development through a loss-of-function mutation. Instead of regulating the developmental program in early embryos where *Btbd18* is highly expressed, BTBD18 controls spermatogenesis by modulating piRNA biogenesis in adult testes.

RESULTS

Apoptotic Cells Appear Late in Meiosis, and Germ Cell Development Is Blocked at the Round Spermatid Stage in *Btbd18* Null Testes

Btbd18 gene encodes an evolutionary conserved protein (Figure S1). We originally focused on BTBD18 and regarded it as a promising reprogramming factor in early embryogenesis because of the high abundance of transcripts in totipotent 2-cell embryos (Figure 1A; see also expression profile in Unigene) and nuclear localization of the protein (Figure S2A). To elucidate its function during development, we generated knockout mice by genetically targeting exon 5 of *Btbd18* to remove most of the coding sequence (Figures S2B and S2C). Heterozygous (+/−) *Btbd18*^{Null} mice generated pups with expected Mendelian ratios (Figure 1B, top panel). Normal-appearing homozygous (−/−) null mice were generated by mating homozygous null females with heterozygous male null mice, which indicates normal embryogenesis in the absence of BTBD18. Unexpectedly, no pups were produced when homozygous null males were co-caged with heterozygous or homozygous null female mice (Figure 1B, bottom panel), demonstrating that *Btbd18* mutant males were sterile. Therefore, we collected testes from control (heterozygous) and *Btbd18*^{Null} (homozygous) males and found that mutant testes were significantly smaller than controls (Figure 1C), suggesting abnormal spermatogenesis. During spermatogenesis, spermatogonia stem cells differentiate into spermatocytes, which meiotically divide into haploid round spermatids to initiate spermiogenesis and form mature spermatozoa. Histological examination demonstrated that genetic ablation of *Btbd18* resulted in post-meiotic blockage at the round spermatid stage with significantly reduced formation of round spermatids (Figures 1D and S2D). TUNEL analysis showed a significant increase in apoptosis within mutant seminiferous tubules (Figure S2E). Further microscopic examination of mutant seminiferous tubules indicated that germ cells become apoptotic from late spermatocyte stage (Figures S2D, 1E, and S2F). Immunostaining of meiotic chromosome spreads of control and *Btbd18*^{Null} spermatocytes confirmed successful synapsis and recombination in absence of BTBD18 (Figure S2G). Because the p53 pathway is often activated to trigger apoptosis in response to stress, we generated *Btbd18*^{Null} mice in a *p53*^{Null} background. However, the failure of spermatogenesis in double-knockout mice (Figure S2H) suggests that p53-independent pathways are involved in germ cell elimination in *Btbd18*^{Null} mice.

BTBD18 Is a Pachytene Nuclear Protein in Mouse Testes

To investigate *Btbd18* gene expression during spermatogenesis, we profiled the major cell types within the testes based on previously reported RNA-sequencing (RNA-seq) data from mice

(Soumillon et al., 2013). We found that *Btbd18* transcripts were consistently present from spermatogonia to spermatids, with trace expression in mature spermatozoa and somatic Sertoli cells (Figure 2A). To further examine developmental expression of the BTBD18 protein, we generated transgenic mice expressing *Btbd18* cDNA with 3.2 kb sequence upstream of the transcription start site as the promoter (Figure 2B). Transgenic BTBD18 was tagged by N-terminal FLAG and C-terminal mCherry for identification. We first documented that expression of the transgene rescues the defect in spermiogenesis and fertility observed in *Btbd18*^{Null} mice (Figures 2C, S3A, and S3B). This indicates that *Btbd18* is specifically targeted in the knockout line and that the *Btbd18*^{FLAG/mCherry} transgene genetically substitutes for the endogenous *Btbd18* gene. We then asked where the BTBD18^{FLAG/mCherry} protein is localized in mouse testes. Although the fluorescent signal was below detection in seminiferous tubules freshly prepared or in frozen testicular sections, immunostaining of frozen testicular sections with anti-mCherry antibody identified specific immunofluorescence in nuclei of pachytene spermatocytes (Figure 2D).

To obtain a global view of developmental localization pattern of BTBD18^{FLAG/mCherry} during spermatogenesis, we prepared frozen sections from *Btbd18*-rescue testes and staged seminiferous tubules based on nuclei morphology and γ H2A.X patterns (Ahmed and de Rooij, 2009; Blanco-Rodriguez, 2009) (Figure S3C). Our staging examination showed that punctate nuclear foci accumulate in early pachytene cells (stages I–VII), decline in late pachytene cells (stages VIII–X), and virtually disappear in diplotene cells (stage XI). Further examination of co-localization of BTBD18^{FLAG/mCherry} and SYCP3 revealed that synaptonemal complexes are juxtaposed between punctate structures of BTBD18 without obvious overlap (Figure 2E). Nor do the punctate nuclear foci co-localize with RNA Pol II (Figure S3D), indicating that BTBD18 is not involved in general transcription events during meiosis. When visualized by immunostaining meiotic chromosome spreads from transgenic testes (Figures 2F and S3E), distinct BTBD18 foci were intriguingly concentrated as “strings” instead of “spots,” with limited numbers adjacent to individual stretches of synaptonemal complexes. Notably, not all chromosomes, in particular sex chromosomes, were labeled by the antibody for BTBD18 identification. Taken together, these results document BTBD18 localization in pachytene nuclei where it binds to discrete chromatin regions within DNA loops or DNA loop-associated subnuclear structures.

Btbd18 Ablation Specifically Reduces the Abundance of a Subset of piRNA Precursor Transcripts

The initial wave of spermatogenesis in mice begins a few days after birth and is synchronous for at least 28 days (Figure 3A). Thus, by collecting postnatal testes from control and *Btbd18*^{Null} mice on different days, we investigated the role of BTBD18 at specific stages of germ cell development. At postnatal day 10 (P10), germ cells have initiated meiosis with spermatocytes appearing but not meiotic pachytene cells. At P14 there are early pachytene cells; at P18, diplotene cells have developed and round spermatids begin to appear; and at P28, spermatozoa are beginning to develop (Bellve et al., 1977). RT-PCR documented that *Btbd18* is expressed in all four stages with a peak

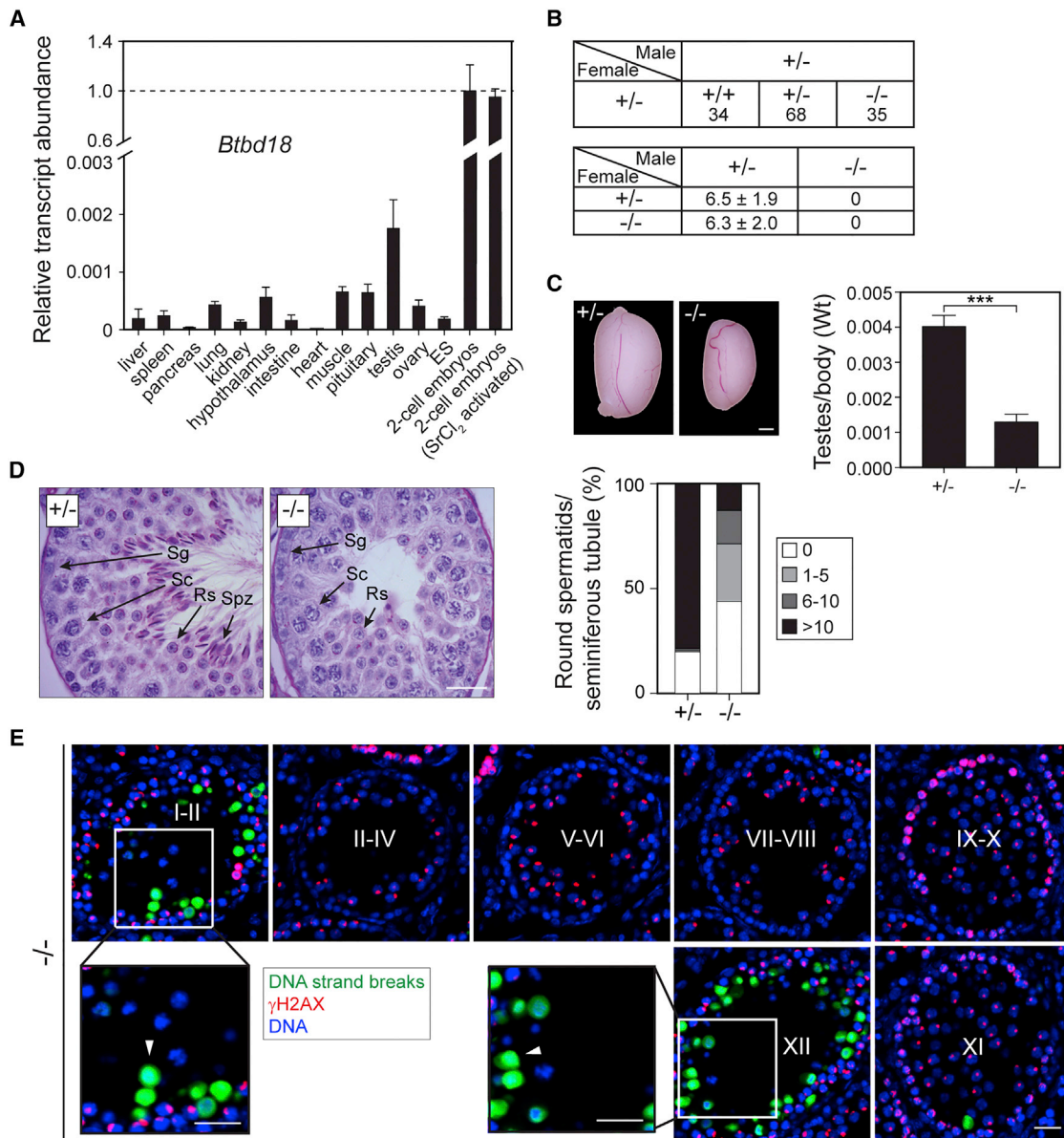


Figure 1. *Btbd18* Is Essential for Spermiogenesis in Mice

(A) Relative abundance of *Btbd18* transcript in adult mouse tissues and early development normalized to abundance at the 2-cell stage, using *Gapdh* transcript as internal control. Error bars denote SD.

(B) Fertility of *Btbd18* knockout mice was determined with 137 pups produced from 21 litters of heterozygous parents (top panel). Mean litter sizes ± SD are shown when co-caged with indicated genotypes (bottom panel). Genotype: +/-, heterozygous; -/-, homozygous.

(C) Images of testes from 8-week-old control (heterozygous) and *Btbd18*^{Null} (homozygous) mice (left). The average ratio of testes to body weight ± SD (right). ****p* < 0.001 by two-tailed Student's *t* test. Scale bar, 2 mm.

(D) Light microscopic images of testes from 4-month-old control (heterozygous) and *Btbd18*^{Null} (homozygous) mice embedded in paraffin, sectioned, and stained with periodic acid-Schiff (PAS)/H&E (left panel). Spermatogonia (Sg), spermatocytes (Sc), round spermatids (Rs), and spermatozoa (Spz) are within seminiferous tubules. Spermatozoa are present in control but not *Btbd18*^{Null} testes and development of round spermatids is arrested at step 3–5. Mean of the percentage of tubules with round spermatids was determined from three biological replicates of control and *Btbd18*^{Null} testes (right panel; at least 400 cross-sections were examined in each sample). Scale bar, 20 μm.

(E) Fluorescent TUNEL staining of sections from 8-week-old homozygous *Btbd18*^{Null} testes. Note that spermatocytes at prophase I are γH2AX positive and negative for DNA strand breaks (terminal deoxynucleotidyl transferase labeling). Arrowhead points to apoptotic primary spermatocytes. Scale bar, 20 μm.

See also [Figures S1](#) and [S2](#).

at P14 ([Figure 3B](#), top panel). TUNEL assay identified elevated cell death in *Btbd18*^{Null} testes from P18 that increased significantly at P28 ([Figure 3B](#), bottom panel; [Figure S4A](#)).

To identify potential downstream targets of *Btbd18*, we isolated poly(A) RNA for RNA-seq from the four developmental stages. Candidate targets were defined after comparing

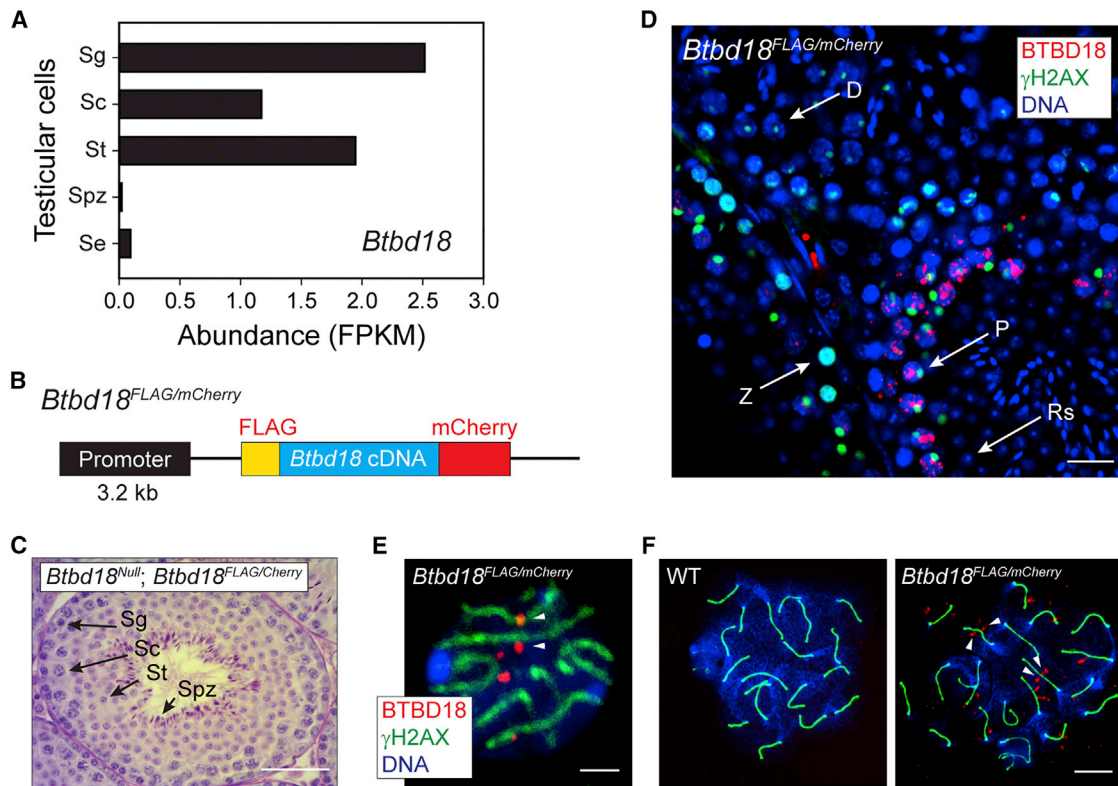


Figure 2. BTBD18 Is Present in Pachytene Nuclei in Adult Mouse Testes

(A) Abundance of *Btbd18* transcripts in testicular cells, including spermatogonia (Sg), spermatocytes (Sc), spermatids (St), spermatozoa (Spz), and Sertoli cells (Se).

(B) Schematic representation of transgenic cassette expressing FLAG-*Btbd18*-mCherry cDNA driven by the *Btbd18* promoter.

(C) Histological sections of testis from *Btbd18*^{Null}; *Btbd18*^{FLAG/mCherry} mice stained with PAS/H&E. Spermatogonia (Sg), spermatocytes (Sc), spermatids (St), and spermatozoa (Spz) are indicated. Scale bar, 50 μ m.

(D) Confocal images of *Btbd18*^{FLAG/mCherry} frozen sections after staining with Hoechst 33342, anti-mCherry, and anti- γ H2A.X antibodies. BTBD18^{FLAG/mCherry} protein localizes in nuclei of pachytene cells and co-stains with γ H2A.X. Zygotene (Z), pachytene (P), diplotene (D) spermatocytes, and round spermatids (Rs) are indicated. Scale bar, 50 μ m.

(E) Frozen sections of *Btbd18*^{FLAG/mCherry} testes stained with Hoechst 33342, anti-mCherry, and anti-SYCP3 antibodies. A representative spermatocyte is shown by arrowheads indicating BTBD18 nuclear localization near stretches of SYCP3 staining of the synaptonemal complex. Scale bar, 2 μ m.

(F) Representative pachytene-stage spermatocyte in meiotic chromosome spreads from control (WT) and *Btbd18*^{FLAG/mCherry} mice. Typical pattern of BTBD18 localization relative to SYCP3 is indicated by arrowheads. Scale bar, 5 μ m.

See also Figure S3.

transcript abundance in control and *Btbd18*^{Null} as those which were more than 2-fold increased or decreased with an adjusted $p < 0.05$ (Figure 3C). A total of 214 piRNA precursors were included with custom annotation using reported genomic locations (Li et al., 2013). Notably, the loss of *Btbd18* had little to no effect on annotated protein-coding genes in P10–P18 testes. However, in P28 testes, of 24,062 genes (a total of 24,276 genes were analyzed including piRNA precursors), 2,528 genes were significantly downregulated and only 107 genes were significantly upregulated. Gene ontology analysis of downregulated genes documented over-representation of genes involved with spermatogenesis and related processes (Figure S4B). Many downregulated genes are highly enriched in spermatids (Soumilion et al., 2013) and are essential for spermatogenesis, including *Chd5* and *Dnmt3l* (Figure S4C). Principal component analysis (PCA) of expressed genes documented gross changes of the transcriptome only at P28 in the absence of BTBD18 protein

(Figure 3D, left panel). These results are in agreement with the observed elimination of spermatids in homozygous *Btbd18*^{Null} testes.

The piRNA precursors in control and *Btbd18*^{Null} testes were similar at P10 (Figure 3C), indicating that pre-pachytene piRNA precursors are not regulated by BTBD18. In *Btbd18*^{Null} testes, seven piRNA precursors were downregulated at P14 and 50 were downregulated at P18, with little further change of piRNA precursors at P28 (Figure 3C). Notably, none of the known piRNA pathway genes (i.e., *A-Myb*, *Miwi*, *Mili*) were changed in P10–P18 testes in absence of BTBD18, and the minimal impact on expression of other protein-coding genes at P10–P18 suggests direct regulation of a subset of piRNA precursors by BTBD18. Almost no piRNA precursors were upregulated at P10–P18 in null mice, indicating that BTBD18 is an activator of piRNA precursors. PCA was also performed for the expression of piRNA precursor genes at the different developmental stages to

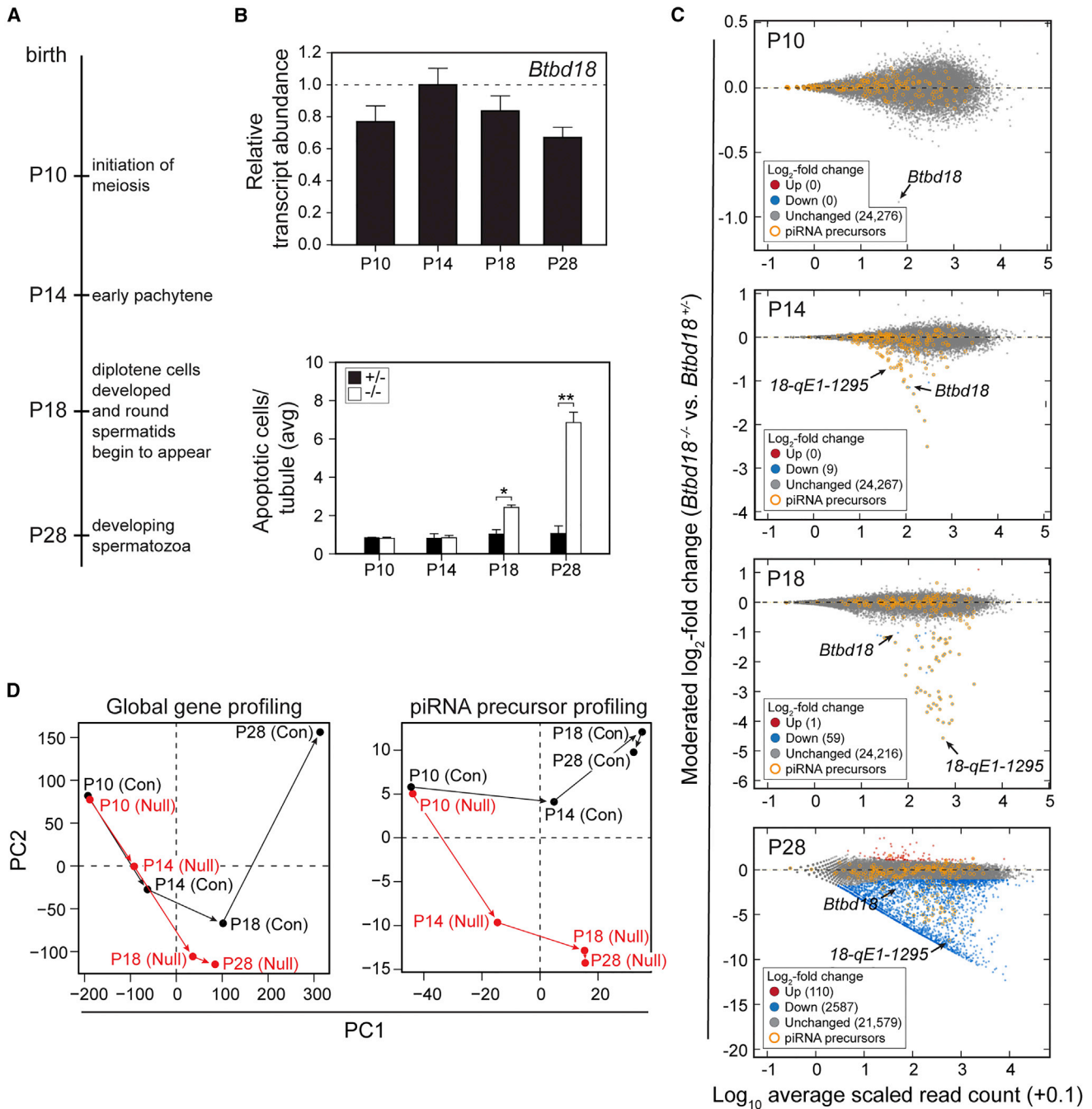


Figure 3. BTBD18 Specifically Activates piRNA Precursors

(A) Timeline for the first postnatal wave of spermatogenesis in mouse testes. P, postnatal day.

(B) Abundance of *Btdb18* transcripts and TUNEL analysis in testes from P10–P28 testes. The highest expression level of *Btdb18* relative to *Gapdh* was set to 1 (top panel). TUNEL-positive cells were quantified in each seminiferous tubule of control (heterozygous) and *Btdb18*^{Null} mice (bottom panel). Mean \pm SD of three independent biological samples. * $p < 0.05$, ** $p < 0.01$ by two-tailed Student's *t* test.

(C) MA plot (log ratio RNA abundance versus abundance) of RNA-seq data comparing control (heterozygous) and *Btdb18*^{Null} (homozygous) testes from P10 to P28. Red and blue dots indicate up- and downregulated genes, respectively. A total of 214 piRNA precursors uniquely mapped onto the mouse genome are circled in yellow. The *Btdb18* gene and one representative downregulated piRNA precursor are indicated.

(D) Principal component (PC) analysis for abundance profiles of global gene (left) or piRNA precursor (right) documented transcriptome correlations among testes isolated at P10–P28 from heterozygous (Con, black) and homozygous *Btdb18*^{Null} (Null, red) mice.

See also Figure S4.

characterize BTBD18 dependency (Figure 3D, right panel). The correlation of altered expression of a subset of piRNA precursor genes at P14 and P18 when pachytene cells appear indicated a regulatory role of BTBD18 at these developmental stages. A Venn diagram of downregulated piRNA precursors demonstrated overlap of dysregulated genes at succeeding stages of development from P14 to P28 (Figure S4D).

There is extensive literature on the role of piRNA biogenesis in preventing mobilization of retrotransposons (Le Thomas et al., 2014; Matranga and Zamore, 2007), particularly members of the *LINE-1* (*L1*) family, to ensure genome integrity in germ cells. However, we did not detect significant changes of *L1* expression in *Btbd18*^{Null} testes (Figure S4E), nor did we detect increased ORF1 protein encoded by the *L1* retrotransposon (Martin and Branciforte, 1993) (Figure S4F). Collectively, these results demonstrate that BTBD18 specifically activates transcription of a set of pachytene piRNA precursors to support developmental program for germ cell development. This is consistent with cellular localization of BTBD18 in mouse testis, which indicates that BTBD18 regulates chromatin events in pachytene cells.

***Btbd18* Deficiency Inhibits piRNA Production from a Subset of Pachytene piRNA Loci**

Among the 214 known piRNA precursors, 50 were downregulated in *Btbd18*^{Null} testes at P18 (Figure 4A). To further investigate BTBD18 function, we divided the piRNA precursors into three populations based on their enrichment in spermatocytes and dependence on BTBD18 for expression: (1) PP-BD (Pachytene piRNA Precursor-BTBD18 Dependent, fold change of expression in spermatocytes versus spermatogonia ≥ 10 and fold change of expression in control versus null ≥ 2); (2) PP-BI (Pachytene piRNA Precursor-BTBD18 Independent, fold change of expression in spermatocytes versus spermatogonia ≥ 10 and fold change of expression in control versus null < 2); (3) PrePP (Pre-Pachytene piRNA Precursor, fold change of expression in spermatocytes versus spermatogonia < 10) (Figure 4B and Table S1). Here, we define PrePP as those piRNA precursors starting to express as early as spermatogonia with some persisting into later stages. Dot-and-box plots on testicular cell types (Soumilion et al., 2013) and developmental stages of testes further confirmed the identities of the three populations (Figures 4C and 4D). We then selected seven precursor genes in three populations and examined the abundance of their transcripts. The expression of each PP-BD genes was downregulated in the absence of *Btbd18* and each recovered expression in rescued testes (Figure S4G). piRNA precursors can be non-coding (nc) or protein-coding (pc) genes (Table S1). Almost all PrePP genes were pc genes (2 nc genes in 99) and almost all PP-BD genes were nc genes (1 pc gene in 50) while PP-BI genes were a mixture of both (48 nc genes and 17 pc genes). The only pc gene in PP-BD category was *Mroh4* (*pi-1700016M24Rik*). The function of *Mroh4* is uncharacterized and ablation of *Mroh4* (Mouse Genome Informatics) documented that homozygous mice were viable and fertile (strain name: C57BL/6N-A^{tm1Brd} *Mroh4*^{tm1a(KOMP)Wtsj}/WtsjH). Despite its unknown functions, *Mroh4* shows testis-specific expression in EST Profile (UniGene) and Gene Expression Atlas (EMBL-EBI). Within testicular cell types, it is enriched in spermatocytes

and spermatids (Figure S4H), which is consistent with its expression being dependent on BTBD18.

To determine whether piRNA production was inhibited by the absence of BTBD18, we collected P10, P14, and P18 testes from control and *Btbd18*^{Null} mice to perform small RNA transcriptome analysis in which β -elimination was used to enrich piRNA populations for deep sequencing (Figures 5A and 5B). Among small RNAs, piRNAs have unique distributions with a uridine bias at their 5' end (Figure S4I). The abundance of piRNAs was normalized to miRNA counts, and we documented that piRNAs derived from PP-BD were specifically decreased in *Btbd18*^{Null} testes (Figures 5C and S4J). Interestingly, piRNA production from protein-coding genes was upregulated in absence of *Btbd18* (Figures S4J and S4K). This indicates inappropriate targeting of piRNA biogenesis machinery to protein-coding genes, which may reflect competition of different transcripts for piRNA biogenesis machinery. Similar phenomena have been reported in *Rnf17*^{Null} (Wasik et al., 2015) and *Mael*^{Null} mice (Castaneda et al., 2014).

These results demonstrate that BTBD18 is specifically involved in primary piRNA biogenesis in the testes, and a null mutation of *Btbd18* impairs expression of a subset of pachytene piRNA precursors and pachytene piRNAs.

BTBD18 Specifically Associates with a Subset of Pachytene piRNA-Producing Loci

Reduced expression of the piRNA precursors and piRNAs may be due to decreased transcription or transcript stability. Therefore, we tested the possibility that BTBD18 regulates transcription by binding to genomic regions of its targeted piRNA precursors. To validate our chromatin immunoprecipitation sequencing (ChIP-seq) conditions, we examined the deposition of A-MYB in testicular cells from 3- to 4-week-old males and confirmed its binding at promoter sequences of pachytene piRNA precursors (Figure 6A). Analysis of differentially expressed genes documented that all 58 downregulated genes in *Btbd18*^{Null} testis at P18 were also significantly repressed in *A-Myb* mutant testis at P17.5 (Figure S5A), but no change was observed in *Btbd18* expression. We then determined the distribution of BTBD18^{FLAG/mCherry} genome wide by ChIP-seq using 3- to 4-week-old BTBD18^{FLAG/mCherry} male testes. ChIP-seq results, using either one or both anti-FLAG and anti-mCherry antibodies, resembled each other in determining BTBD18 enrichment at genomic loci of the three populations of piRNA precursors (Figures 6B and S5B). ChIP-seq results using both antibodies provided the highest signal-to-noise ratio by visual inspection, and therefore were used for further analysis.

Peak density plots show that BTBD18 is enriched immediately downstream of the transcription start sites (TSSs) of PP-BD, but not PP-BI or PrePP genes, and extends into the rest of the loci before diminishing (Figure 6B). In fly ovaries, the Rhino complex binds to fly-specific heterochromatic piRNA clusters and suppresses splicing of piRNA cluster transcripts (Mohn et al., 2014; Zhang et al., 2014b). In contrast, no obvious changes of splicing events were observed at genomic loci of PP-BD genes in the absence of BTBD18 by visual inspection of RNA-seq datasets.

We employed PePr and MACS2 algorithms to identify BTBD18 peaks throughout the mouse genome (Figures 6C and

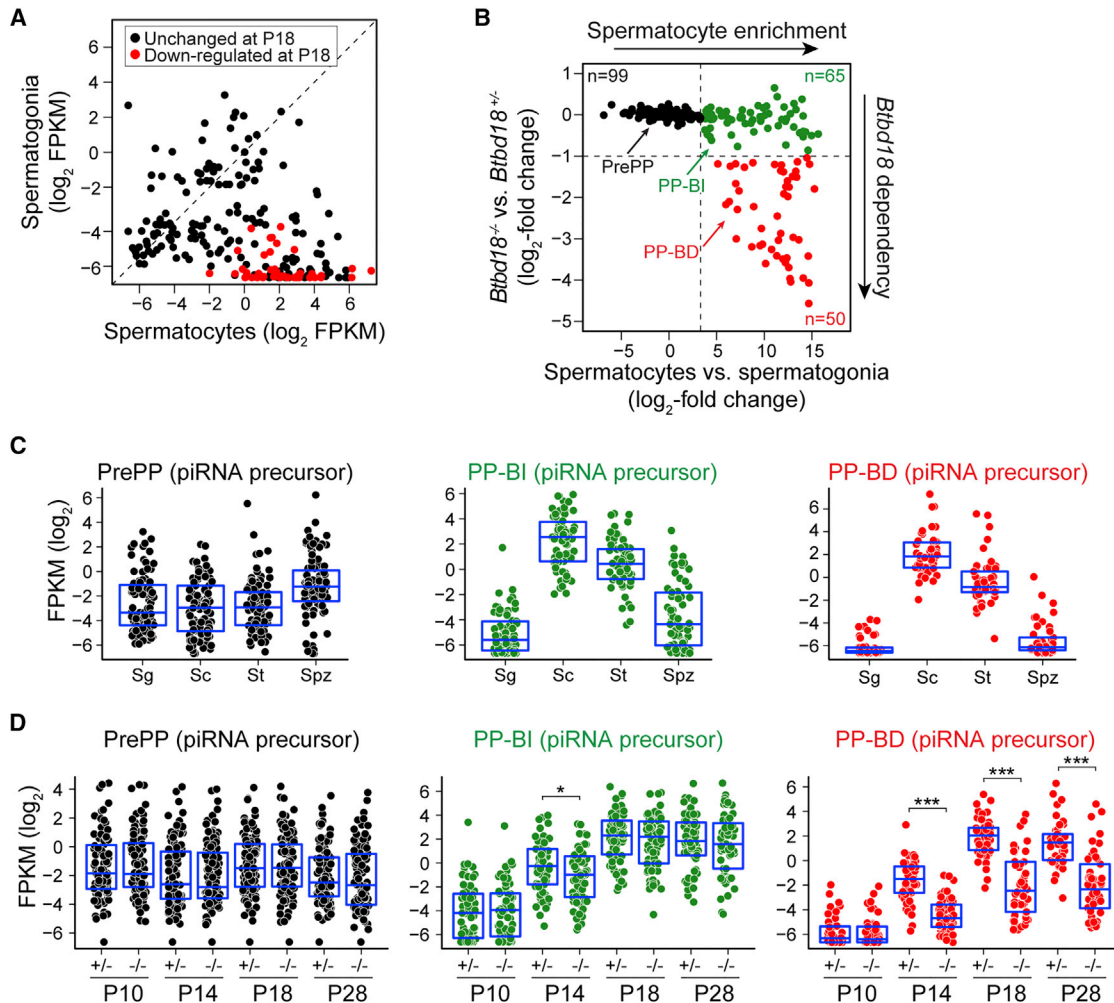


Figure 4. BTBD18 Regulates Biogenesis of a Subset of Pachytene piRNA Precursors

(A) Scatterplot of expression of 214 piRNA precursors in spermatogonia and spermatocytes. piRNA precursors downregulated in P18 testes are indicated as red dots and the rest as black dots.

(B) Scatterplot of piRNA precursor dependence on BTBD18 and enrichment in spermatocytes. Fold change was calculated by DESeq2. Three populations (PrePP, PP-BI, PP-BD) are shown as black, green, and red dots, respectively, with gene numbers for each population indicated in the corresponding color. PrePP, pre-pachytene piRNA precursor; PP-BI, pachytene piRNA precursor BTBD18 independent; PP-BD, pachytene piRNA precursor BTBD18 dependent.

(C) Dot-and-box plots of abundance (log₂ FPKM [fragments per kilobase of exon per million mapped reads]) of three piRNA precursor populations: PrePP (black, left), PP-BI (green, middle), PP-BD (red, right) in different germ cells. Sg, spermatogonia; Sc, spermatocytes; St, spermatids; Spz, spermatozoa.

(D) Dot-and-box plots of abundance (log₂ FPKM) of the three piRNA precursor populations in control (heterozygous) and *Btbd18*^{Null} (homozygous) testes from P10 to P28. *p < 0.05, ***p < 0.001 by Wilcoxon rank-sum test.

See also Figure S4 and Table S1.

6D; Table S2). The PePr algorithm identified 80 unique genomic sites with most of them (73 sites) overlapping with PP-BD loci. A few (three sites) overlapped with PP-BI loci and an additional four sites mapped to unannotated genomic regions. The MACS2 algorithm identified 135 unique genomic sites with most of them (86 sites) overlapping with PP-BD loci and a few (six sites) with PP-BI loci. Additional sites (nine sites) mapped to piRNA-producing protein-coding genes and the rest (34 sites) to unannotated regions. To account for the BTBD18 peaks at unannotated regions, we reviewed our ChIP-seq, RNA-seq, and piRNA profiles by visual inspection. Six peaks identified by MACS2 (labeled in Table S2) were considered binding artifacts because

corresponding peaks were also present in the input sample (Carroll et al., 2014). Consistent with this designation, there was neither gene transcription or piRNA production and no A-MYB occupancy near the sites (Figure 6D, right panel). In contrast, all other unannotated peak regions identified by PePr and MACS2 were transcribed, generated piRNA, and co-localized with A-MYB peaks (Figure 6D, middle panel). Additionally the nine sites identified by MACS2 at protein-coding genes have A-MYB binding and piRNA production. Therefore, we propose that BTBD18 specifically binds to a subset of piRNA loci in the testis, and our results strongly indicate that BTBD18 occupancy directly activates expression of piRNA precursors. The

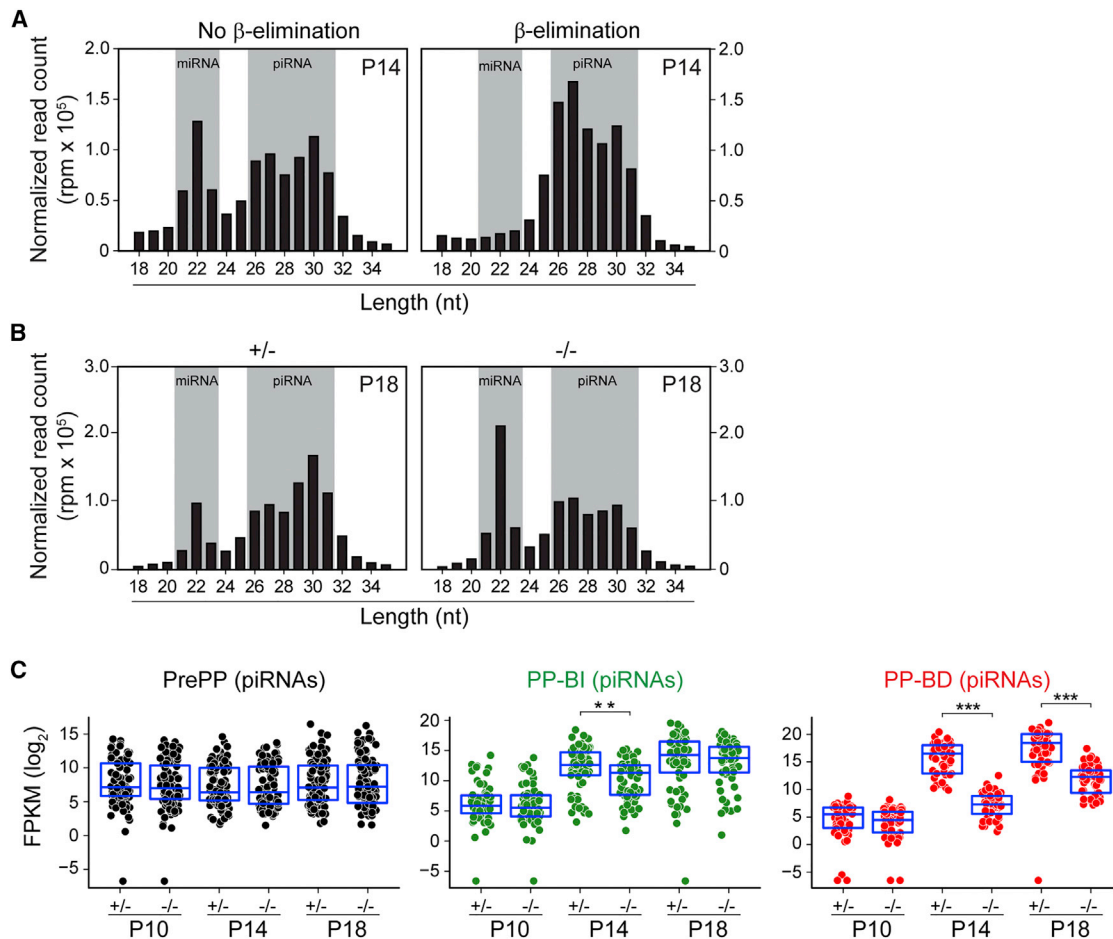


Figure 5. BTBD18 Regulates Pachytene piRNA Biogenesis

(A) Length distribution of small RNA-seq reads with or without β -elimination in P14 control testes, normalized by library size. miRNA (21–23 nt) and piRNA (26–31 nt) populations are highlighted in gray.

(B) Length distribution of small RNA-seq reads in P18 control (heterozygous) and *Btd18*^{Null} (homozygous) testes, normalized by library size. miRNA and piRNA populations are highlighted in gray.

(C) Dot-and-box plots of piRNA abundance (\log_2 FPKM) from PrePP (black, left), PP-BI (green, middle), and PP-BD (red, right) loci in control (heterozygous) and *Btd18*^{Null} (homozygous) testes from P10 to P18. piRNA expression level was normalized to total miRNA reads. **p < 0.01, ***p < 0.001 by Wilcoxon rank-sum test.

See also Figure S4.

co-localization of A-MYB binding sites with piRNA precursors (Figure 6C), supports the remarkable specificity of BTBD18 occupancy at a subset of, although not all, genomic piRNA loci.

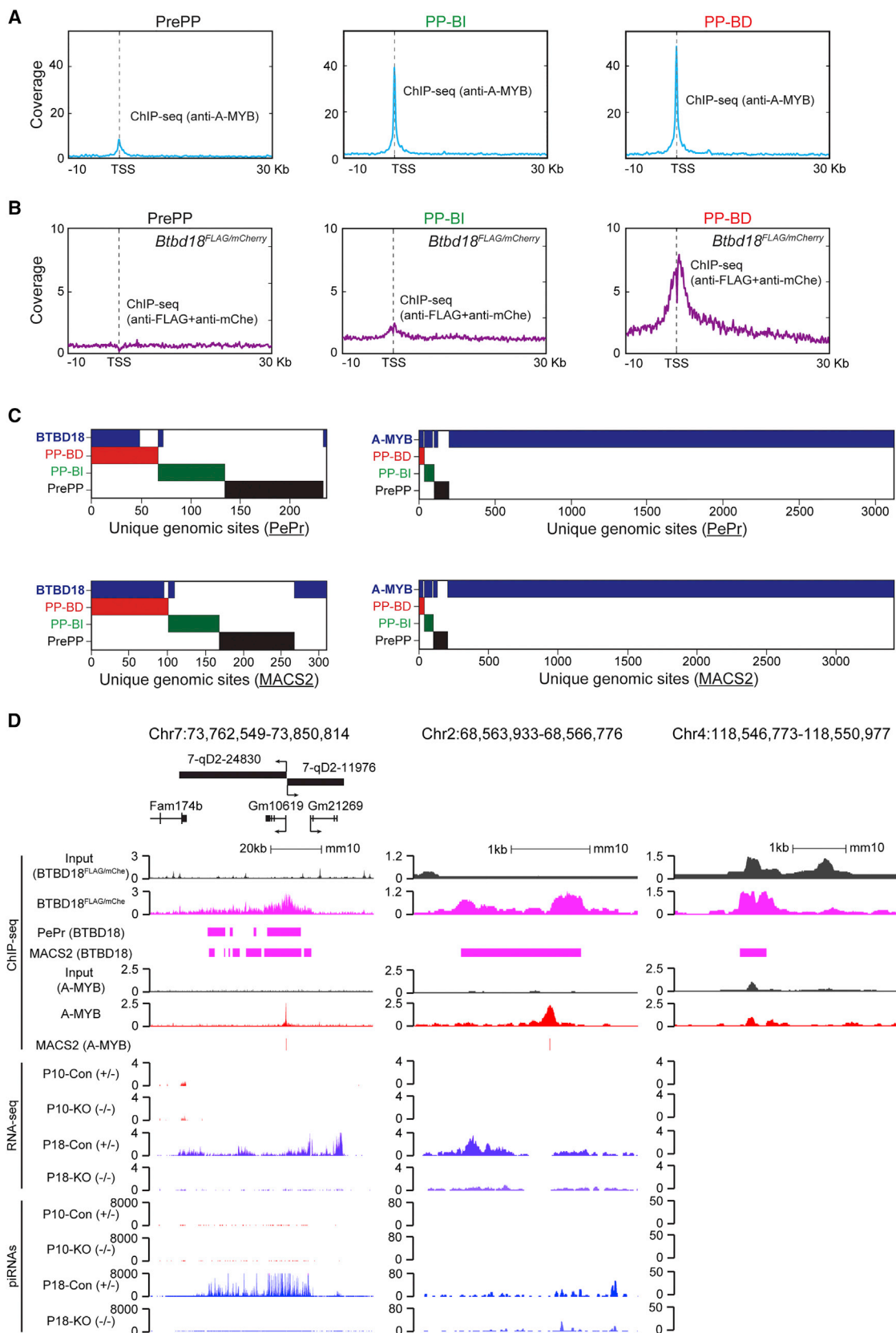
Taken together, our results show that BTBD18 specifically aggregates at a subset of pachytene piRNA-producing loci, and its spread along the entire loci functionally correlates with piRNA precursor expression as well as piRNA production.

BTBD18 Facilitates Transcription Elongation at Pachytene piRNA Loci

During spermatogenesis, piRNAs are generated with various populations at different developmental stages (Gan et al., 2011). The differentiation of these cell types is associated with changes in gene expression and the underlying chromatin landscape. To gain further mechanistic insight into BTBD18 regulation of piRNA precursors, we conducted fluorescence-activated

cell sorting (FACS) to isolate spermatocytes and round spermatids from testicular cells of control and *Btd18*^{Null} males, followed by analyses of their transcriptomes and epigenomes. In these studies, germ cells were genetically labeled by *Stra8*-iCre triggered enhanced yellow fluorescent protein (EYFP) (Figure 7A) to facilitate Hoechst 33342-based flow cytometry for cell sorting (Figure 7B).

For transcriptome analysis, we performed strand-specific RNA-seq to compare gene expression in control and *Btd18*^{Null} spermatocytes/round spermatids (Figure 7C). In agreement with RNA-seq results in testes, we documented that PP-BD genes were significantly downregulated in *Btd18*^{Null} spermatocytes and spermatids. No significant change was observed in PrePP and PP-BI genes in spermatocytes. However, for reasons that remain unclear, PrePP genes were upregulated and PP-BI genes were downregulated in spermatids, which may reflect



(legend on next page)

downstream events of changed piRNA profiles in *Btbd18*^{Null} spermatocytes or different cell populations in *Btbd18*^{Null} spermatids.

To determine how BTBD18 regulates transcription of its targeted piRNA precursors, we investigated chromatin structure at these genomic loci. To measure changes of chromatin accessibility, we performed assay for transposase-accessible chromatin sequencing (ATAC-seq) on freshly isolated spermatocytes (Figure 7D). In control spermatocytes, a sharp peak centered on the TSS of pachytene piRNA precursors was always present, followed by a broad peak into the transcription unit. In the absence of BTBD18, formation of an accessible chromatin structure at gene bodies of PP-BD genes was severely disrupted, which supports a role for BTBD18 in regulating transcription activity rather than transcript stability. However, chromatin regions around the TSS of PP-BD genes were still accessible despite the loss of BTBD18, suggesting regulatory roles of BTBD18 in assembly of the transcription machinery after promoter opening. Therefore, we performed ChIP-seq analysis to profile Pol II occupancy in control and *Btbd18*^{Null} testicular cells (Figure 7E). In agreement with ATAC-seq results, extension of Pol II in PP-BD loci was significantly restricted to genomic regions around the TSSs in the absence of BTBD18 (Figure 7F), indicating non-productive elongation. This result documents the existence of a 5' checkpoint as Pol II moves away from the promoters of piRNA precursors during early elongation, with transcription halted without a proper licensing signal by BTBD18.

Thus, we conclude that BTBD18 acts after Pol II recruitment and enforces transcription elongation in open chromatin structures to ensure maximal expression of a subset of pachytene piRNA precursors for developmental programs in mouse testes.

DISCUSSION

piRNAs are produced from discrete genomic loci of large transcribed clusters with unclear chromatin signatures. Here, we demonstrate that BTBD18 acts as a specified transcription activator of a subset of pachytene piRNAs in mouse testes. Disruption of BTBD18 significantly reduced expression of primary piRNA precursors and severely impaired piRNA production. We further found that BTBD18 directly occupies discrete genomic loci of these piRNA precursors to promote transcription elongation. Although mice lacking BTBD18 initiate spermatogenesis, many spermatocytes are lost by apoptosis and arrested spermiogenesis results in azoospermia and male infertility.

BTBD18 Regulates a Subset of Pachytene piRNA Precursor Transcripts Necessary for Spermiogenesis

Genetic ablation of *Btbd18* causes massive apoptosis at the late spermatocyte stage and developmental arrest at the haploid round spermatid stage of spermatogenesis. This phenotype resembles mutation of other piRNA pathway genes including *Miwi*, a member of the *Piwi* family of Argonaute genes (Deng and Lin, 2002). MIWI protein plays an essential role in processing piRNA precursors into mature piRNA, and *L1* retrotransposons are derepressed in *Miwi* mutant testes because of reduced piRNAs derived from retrotransposon fragments (Reuter et al., 2011). A similar phenotype has been reported for *Mael*^{Null} mice spermiogenic arrest attributed to derepressed *L1* expression and significant reduced translation of spermiogenic mRNAs (Castaneda et al., 2014). These observations suggest that the absence of BTBD18 may adversely affect translation due to changed piRNA production from non-coding and protein-coding precursors, which ultimately leads to spermiogenic arrest. Whether this reflects targeting specific RNAs or a more global degradation of RNA remains to be determined. Notably, the absence of retrotransposon upregulation in *Btbd18*^{Null} testis suggests that its effect on transcription provides regulation of more restricted piRNA populations than does the post-transcriptional regulation observed in the *Miwi*^{Null} and *Mael*^{Null} mice. The dramatic effect on spermiogenesis in the absence of retrotransposon derepression in *Btbd18*^{Null} mice raises the possibility of targeting BTBD18 protein for male contraception.

Propagation and Regulation of a Subset of piRNA Loci by BTBD18

How BTBD18 acquires its specificity for a subset of pachytene piRNA-producing loci to regulate chromatin structure needs further exploration. Currently, most chromatin regulators in testes demonstrate broader target specificity than piRNA-producing loci. For example, A-MYB is a well-known transcription factor that targets piRNA loci but also targets meiotic genes (Li et al., 2013). Therefore, other unknown factors must exist to restrict chromatin binding of BTBD18 to a limited number of genomic loci.

Combinatorial interactions of multiple transcription factors may define the promoter area of a subset of piRNA loci and guide recruitment of BTBD18 elongation complex followed by BTBD18 spreading along the transcriptional unit. Beyond A-MYB noted above, we have analyzed chromatin occupancy profiles of other transcription factors (Figure S6A) and identified biased binding patterns among the three defined populations of piRNA precursors (PrePP, PP-BI, PP-BD). TAF7L binds strongly to PrePP

Figure 6. BTBD18 Occupies Pachytene piRNA-Generating Loci

(A) Read density profiles (deepTools normalized coverage) of ChIP-seq for PrePP, PP-BI, and PP-BD populations with anti-A-MYB antibody in 100-bp bins, using *Btbd18*^{-/-} testes. TSS, transcription start site.

(B) Same as (A), but with two antibodies (anti-FLAG and anti-mCherry) for ChIP-seq of BTBD18.

(C) Binary heatmap depicting overlap of BTBD18 (left) or A-MYB (right) binding sites (blue) with unique genomic sites of PP-BD (red), PP-BI (green), and PrePP (black), using either PePr (top) or MACS2 (bottom) algorithms for peak calling. Genomic regions of piRNA precursors were expanded by 2 kb upstream of TSS to test the overlap of A-MYB occupancy with piRNA loci.

(D) UCSC Genome Browser screenshot of ChIP-seq signals, RNA-seq signals and piRNA profiles at the genomic region of 7-qD2-24830 and 7-qD2-11976 (left, a transcribed PP-BD gene pair), a representative unannotated piRNA locus on chromosome 2 (middle), and a representative unannotated region in chromosome 4 (right, considered as artifact as noted in text). Identified peaks by PePr and MACS2 are shown below ChIP-seq profiles. ChIP-seq signals are displayed as RPM (reads per million reads) values, and RNA-seq signals and piRNA profiles are displayed as normalized value of coverage by size factor.

See also Figure S5 and Table S2.

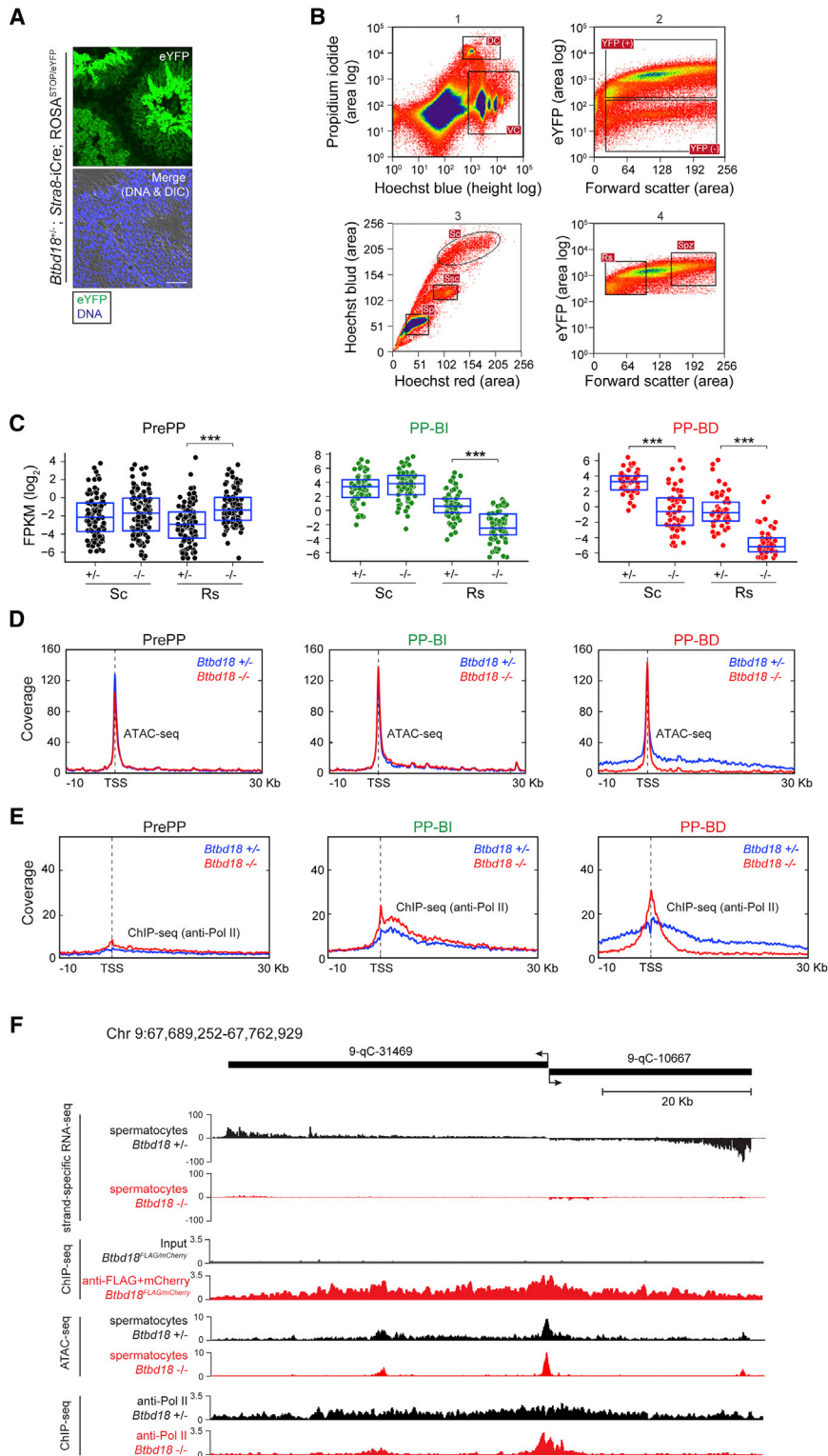


Figure 7. BTBD18 Promotes Transcription Elongation at a Subset of Pachytene piRNA-Generating Loci

(A) Labeling of testicular cells. Confocal microscopy of frozen testicular sections from *Btb18*^{+/-}; *Stra8*-*iCre*; *ROSA*^{Stop/eYFP} mice with germ cells labeled by EYFP. Scale bar, 50 μ m.

(B) Purification of testicular cells. Spermatocytes (Sc) and round spermatids (Rs) were isolated by FACS using the indicated gate settings. DC, dead cells; VC, viable cells; Ssc, secondary spermatocytes; St, spermatids; Spz, spermatozoa.

(C) Dot-and-box plots of piRNA abundance (\log_2 FPKM) of PrePP (black, left panel), PP-BI (green, middle panel), and PP-BD (red, right panel) in FACS-purified spermatocytes (Sc) and round spermatids (Rs) from control (heterozygous, +/-) and *Btb18*^{Null} (homozygous, -/-) testes of 4-month-old mice. *** $p < 0.001$ by Wilcoxon rank-sum test.

(D) Read density profiles of ATAC-seq for PrePP, PP-BI, and PP-BD populations from control (blue, heterozygous) and *Btb18*^{Null} (red, homozygous) spermatocytes in 100-bp bins.

(E) Read density profiles of ChIP-seq displaying chromatin occupancy of Pol II relative to TSS of PrePP, PP-BI, and PP-BD populations in control (blue, heterozygous) and *Btb18*^{Null} (red, homozygous) testes in 100-bp bins.

(F) UCS Genomic Browser screenshot of strand-specific RNA-seq, ATAC-seq, and ChIP-seq of Pol II in the presence or absence of BTBD18 at the genomic region of 9-qC-31469 and 9-qC-10667 (a \sim 70kb transcribed PP-BD gene pair) with a bidirectional promoter. Occupancy of BTBD18 is also shown by ChIP-seq. ChIP-seq and ATAC-seq signals are displayed as RPM values, and RNA-seq signals and piRNA profiles are displayed as normalized value of coverage by size factor. See also Figure S6.

also may be structural motifs in the 5' end of nascent piRNA precursor transcripts (Homolka et al., 2015; Ishizu et al., 2015) creating chromatin structures of the cognate genomic loci co-transcriptionally (Yu et al., 2015) to facilitate recruitment of the BTBD18-containing protein complex. How BTBD18 spreads across the entire loci of its targets remains unclear, but may involve self-association through its BTB domain.

Different response of piRNA precursors to BTBD18 suggests differential chromatin signatures and transcriptional control at discrete piRNA loci. We have investigated different histone modifica-

promoters, which correlates with open chromatin structure (Figure 7D) despite negligible expression of PrePP genes (Figures 4D and 7C) (Zhou et al., 2013). Notably, RFX2 has biased binding at PP-BD promoters, and *RFX2*^{Null} mice, which are viable, are sterile due to spermiogenic arrest (Kistler et al., 2015). There

are also structural motifs in the 5' end of nascent piRNA precursor transcripts (Homolka et al., 2015; Ishizu et al., 2015) creating chromatin structures of the cognate genomic loci co-transcriptionally (Yu et al., 2015) to facilitate recruitment of the BTBD18-containing protein complex. How BTBD18 spreads across the entire loci of its targets remains unclear, but may involve self-association through its BTB domain. Different response of piRNA precursors to BTBD18 suggests differential chromatin signatures and transcriptional control at discrete piRNA loci. We have investigated different histone modifica-

be interesting to determine whether and how BTBD18 interacts with these modifications. In addition, BTB-containing proteins are known to interact with cullin to assemble E3 ligases and mediate protein ubiquitination (Perez-Torrado et al., 2006). This raises the possibility that BTBD18 may also mediate histone H2B ubiquitination to promote RNA Pol II elongation (Weake and Workman, 2008).

In summary, our data demonstrate that BTBD18 occupies a subset of pachytene piRNA-producing loci and supports transcription activity for piRNA biogenesis, thereby orchestrating developmental programming in mouse testes to ensure successful germ cell production.

STAR★METHODS

Detailed methods are provided in the online version of this paper and include the following:

- KEY RESOURCES TABLE
- CONTACT FOR REAGENT AND RESOURCE SHARING
- EXPERIMENTAL MODEL AND SUBJECT DETAILS
- METHOD DETAILS
 - Mice
 - Histology Examination
 - Preparation of Testicular Frozen Sections for Immunofluorescence
 - Meiotic Chromosome Spreads for Immunofluorescence
 - Realtime RT-PCR
 - Fluorescence-Activated Cell Sorting (FACS)
 - RNA-Seq Library Preparation
 - Small RNA-Seq Library Preparation
 - ChIP-Seq Library Preparation
 - ATAC-Seq Library Preparation
 - Common Library Analyses
- QUANTIFICATION AND STATISTICAL ANALYSIS
 - RNA-Seq Data Analysis
 - Small RNA-Seq Data Analysis
 - ChIP-Seq and ATAC-Seq Data Analysis
 - Statistical Analysis
- DATA AND SOFTWARE AVAILABILITY

SUPPLEMENTAL INFORMATION

Supplemental Information includes six figures and three tables and can be found with this article online at <http://dx.doi.org/10.1016/j.devcel.2017.02.007>.

AUTHOR CONTRIBUTIONS

L.Z. and J.D. designed the experiments, analyzed the data, and wrote the paper. L.Z. performed the experiments. B.C. performed bioinformatics analysis. Y.Z. and L.Z. performed mouse embryonic stem cell targeting. Y.Z. performed embryonic stem cell injection and prepared frozen sections. B.B. and L.Z. performed microscopic analyses. K.T. and L.Z. performed morphology examination. D.M. performed FACS analysis.

ACKNOWLEDGMENTS

We thank all members of J.D.'s laboratory for helpful suggestions on the project. We thank Dr. R. Daniel Camerini-Otero's laboratory (NIDDK) for advice on meiosis and morphology. We thank Dr. Astrid D. Haase (NIDDK) and her

laboratory member Dr. Pavol Genzor for helpful discussion on the project. We thank Dr. Alex Bortvin (Carnegie Institution for Science) for providing anti-ORF1p antibody. We thank Dr. Chul Min Yang (NIDDK) for help with the ATAC-seq experiment. We thank Dr. Chengyu Liu's laboratory (NHLBI) for technical advice and assistance with mouse genetics. We thank the NIDDK Genomics Core for deep sequencing, and the NIH HPC Biowulf cluster for high-performance computing. This research was supported by the Intramural Research Program of the NIH, The National Institute of Diabetes and Digestive and Kidney Disease (NIDDK).

Received: June 14, 2016

Revised: November 18, 2016

Accepted: February 9, 2017

Published: March 13, 2017

REFERENCES

- Ahmed, E.A., and de Rooij, D.G. (2009). Staging of mouse seminiferous tubule cross-sections. *Methods Mol. Biol.* 558, 263–277.
- Aravin, A.A., and Hannon, G.J. (2008). Small RNA silencing pathways in germ and stem cells. *Cold Spring Harb Symp. Quant. Biol.* 73, 283–290.
- Aravin, A., Gaidatzis, D., Pfeffer, S., Lagos-Quintana, M., Landgraf, P., Iovino, N., Morris, P., Brownstein, M.J., Kuramochi-Miyagawa, S., Nakano, T., et al. (2006). A novel class of small RNAs bind to MILI protein in mouse testes. *Nature* 442, 203–207.
- Bellve, A.R., Cavicchia, J.C., Millette, C.F., O'Brien, D.A., Bhatnagar, Y.M., and Dym, M. (1977). Spermatogenic cells of the prepubertal mouse. Isolation and morphological characterization. *J. Cell Biol.* 74, 68–85.
- Blanco-Rodriguez, J. (2009). gammaH2AX marks the main events of the spermatogenic process. *Microsc. Res. Tech.* 72, 823–832.
- Bolcun-Filas, E., Bannister, L.A., Barash, A., Schimenti, K.J., Hartford, S.A., Eppig, J.J., Handel, M.A., Shen, L., and Schimenti, J.C. (2011). A-MYB (MYBL1) transcription factor is a master regulator of male meiosis. *Development* 138, 3319–3330.
- Buenrostro, J.D., Giresi, P.G., Zaba, L.C., Chang, H.Y., and Greenleaf, W.J. (2013). Transposition of native chromatin for fast and sensitive epigenomic profiling of open chromatin, DNA-binding proteins and nucleosome position. *Nat. Methods* 10, 1213–1218.
- Buenrostro, J.D., Wu, B., Chang, H.Y., and Greenleaf, W.J. (2015). ATAC-seq: a method for assaying chromatin accessibility genome-wide. *Curr. Protoc. Mol. Biol.* 109, 21.29.1–21.29.9.
- Carroll, T.S., Liang, Z., Salama, R., Stark, R., and de Santiago, I. (2014). Impact of artifact removal on ChIP quality metrics in ChIP-seq and ChIP-exo data. *Front. Genet.* 5, 75.
- Castaneda, J., Genzor, P., van der Heijden, G.W., Sarkeshik, A., Yates, J.R., 3rd, Ingolia, N.T., and Bortvin, A. (2014). Reduced pachytene piRNAs and translation underlie spermiogenic arrest in Maelstrom mutant mice. *EMBO J.* 33, 1999–2019.
- Chang, Y.F., Lee-Chang, J.S., Panneerdoss, S., MacLean, J.A., 2nd, and Rao, M.K. (2011). Isolation of Sertoli, Leydig, and spermatogenic cells from the mouse testis. *Biotechniques* 51, 341–342, 344.
- Criscione, S.W., Zhang, Y., Thompson, W., Sedivy, J.M., and Neretti, N. (2014). Transcriptional landscape of repetitive elements in normal and cancer human cells. *BMC Genomics* 15, 583.
- De Fazio, S., Bartonicek, N., Di Giacomo, M., Abreu-Goodger, C., Sankar, A., Funaya, C., Antony, C., Moreira, P.N., Enright, A.J., and O'Carroll, D. (2011). The endonuclease activity of Mili fuels piRNA amplification that silences LINE1 elements. *Nature* 480, 259–263.
- Deng, W., and Lin, H. (2002). miwi, a murine homolog of piwi, encodes a cytoplasmic protein essential for spermatogenesis. *Dev. Cell* 2, 819–830.
- Eden, E., Navon, R., Steinfeld, I., Lipson, D., and Yakhini, Z. (2009). GOrilla: a tool for discovery and visualization of enriched GO terms in ranked gene lists. *BMC Bioinformatics* 10, 48.

- Gan, H., Lin, X., Zhang, Z., Zhang, W., Liao, S., Wang, L., and Han, C. (2011). piRNA profiling during specific stages of mouse spermatogenesis. *RNA* 17, 1191–1203.
- Girard, A., Sachidanandam, R., Hannon, G.J., and Carmell, M.A. (2006). A germline-specific class of small RNAs binds mammalian Piwi proteins. *Nature* 442, 199–202.
- Goh, W.S., Falcatori, I., Tam, O.H., Burgess, R., Meikar, O., Kotaja, N., Hammell, M., and Hannon, G.J. (2015). piRNA-directed cleavage of meiotic transcripts regulates spermatogenesis. *Genes Dev.* 29, 1032–1044.
- Gou, L.T., Dai, P., Yang, J.H., Xue, Y., Hu, Y.P., Zhou, Y., Kang, J.Y., Wang, X., Li, H., Hua, M.M., et al. (2015). Pachytene piRNAs instruct massive mRNA elimination during late spermiogenesis. *Cell Res.* 25, 266.
- Hammoud, S.S., Low, D.H., Yi, C., Carrell, D.T., Guccione, E., and Cairns, B.R. (2014). Chromatin and transcription transitions of mammalian adult germline stem cells and spermatogenesis. *Cell Stem Cell* 15, 239–253.
- Homolka, D., Pandey, R.R., Goriaux, C., Brasset, E., Vaury, C., Sachidanandam, R., Fauvarque, M.O., and Pillai, R.S. (2015). PIWI slicing and RNA elements in precursors instruct directional primary piRNA biogenesis. *Cell Rep.* 12, 418–428.
- Ishizu, H., Iwasaki, Y.W., Hirakata, S., Ozaki, H., Iwasaki, W., Siomi, H., and Siomi, M.C. (2015). Somatic primary piRNA biogenesis driven by cis-acting RNA elements and trans-acting Yb. *Cell Rep.* 12, 429–440.
- Kim, D., Perte, G., Trapnell, C., Pimentel, H., Kelley, R., and Salzberg, S.L. (2013). TopHat2: accurate alignment of transcriptomes in the presence of insertions, deletions and gene fusions. *Genome Biol.* 14, R36.
- Kistler, W.S., Baas, D., Lemeille, S., Paschaki, M., Seguin-Estevez, Q., Barras, E., Ma, W., Duteyrat, J.L., Morle, L., Durand, B., et al. (2015). RFX2 is a major transcriptional regulator of spermiogenesis. *PLoS Genet.* 11, e1005368.
- Langmead, B., Trapnell, C., Pop, M., and Salzberg, S.L. (2009). Ultrafast and memory-efficient alignment of short DNA sequences to the human genome. *Genome Biol.* 10, R25.
- Lau, N.C., Seto, A.G., Kim, J., Kuramochi-Miyagawa, S., Nakano, T., Bartel, D.P., and Kingston, R.E. (2006). Characterization of the piRNA complex from rat testes. *Science* 313, 363–367.
- Le Thomas, A., Toth, K.F., and Aravin, A.A. (2014). To be or not to be a piRNA: genomic origin and processing of piRNAs. *Genome Biol.* 15, 204.
- Li, X.Z., Roy, C.K., Dong, X., Bolcun-Filas, E., Wang, J., Han, B.W., Xu, J., Moore, M.J., Schimmler, J.C., Weng, Z., et al. (2013). An ancient transcription factor initiates the burst of piRNA production during early meiosis in mouse testes. *Mol. Cell* 50, 67–81.
- Love, M.I., Huber, W., and Anders, S. (2014). Moderated estimation of fold change and dispersion for RNA-seq data with DESeq2. *Genome Biol.* 15, 550.
- Martin, S.L., and Branciforte, D. (1993). Synchronous expression of LINE-1 RNA and protein in mouse embryonal carcinoma cells. *Mol. Cell. Biol.* 13, 5383–5392.
- Matranga, C., and Zamore, P.D. (2007). Small silencing RNAs. *Curr. Biol.* 17, R789–R793.
- Mei, S., Qin, Q., Wu, Q., Sun, H., Zheng, R., Zang, C., Zhu, M., Wu, J., Shi, X., Taing, L., et al. (2017). Cistrome Data Browser: a data portal for ChIP-seq and chromatin accessibility data in human and mouse. *Nucleic Acids Res.* 45, D658–D662.
- Mohn, F., Sienski, G., Handler, D., and Brennecke, J. (2014). The rhino-deadlock-cutoff complex licenses noncanonical transcription of dual-strand piRNA clusters in *Drosophila*. *Cell* 157, 1364–1379.
- Muerdter, F., Olovnikov, I., Molaro, A., Rozhkov, N.V., Czech, B., Gordon, A., Hannon, G.J., and Aravin, A.A. (2012). Production of artificial piRNAs in flies and mice. *RNA* 18, 42–52.
- Perez-Torrado, R., Yamada, D., and Defossez, P.A. (2006). Born to bind: the BTB protein-protein interaction domain. *BioEssays* 28, 1194–1202.
- Ramirez, F., Dundar, F., Diehl, S., Gruning, B.A., and Manke, T. (2014). deepTools: a flexible platform for exploring deep-sequencing data. *Nucleic Acids Res.* 42, W187–W191.
- Reuter, M., Berninger, P., Chuma, S., Shah, H., Hosokawa, M., Funaya, C., Antony, C., Sachidanandam, R., and Pillai, R.S. (2011). Miwi catalysis is required for piRNA amplification-independent LINE1 transposon silencing. *Nature* 480, 264–267.
- Robine, N., Lau, N.C., Balla, S., Jin, Z., Okamura, K., Kuramochi-Miyagawa, S., Blower, M.D., and Lai, E.C. (2009). A broadly conserved pathway generates 3'UTR-directed primary piRNAs. *Curr. Biol.* 19, 2066–2076.
- Roovers, E.F., Rosenkranz, D., Mahdipour, M., Han, C.T., He, N., Chuva de Sousa Lopes, S.M., van der Westerlaken, L.A., Zischler, H., Butter, F., Roelen, B.A., et al. (2015). Piwi proteins and piRNAs in mammalian oocytes and early embryos. *Cell Rep.* 10, 2069–2082.
- Saxe, J.P., Chen, M., Zhao, H., and Lin, H. (2013). Tdrkh is essential for spermatogenesis and participates in primary piRNA biogenesis in the germline. *EMBO J.* 32, 1869–1885.
- Sin, H.S., Kartashov, A.V., Hasegawa, K., Barski, A., and Namekawa, S.H. (2015). Poised chromatin and bivalent domains facilitate the mitosis-to-meiosis transition in the male germline. *BMC Biol.* 13, 53.
- Soper, S.F., van der Heijden, G.W., Hardiman, T.C., Goodheart, M., Martin, S.L., de Boer, P., and Bortvin, A. (2008). Mouse maelstrom, a component of nuage, is essential for spermatogenesis and transposon repression in meiosis. *Dev. Cell* 15, 285–297.
- Soumillon, M., Necsulea, A., Weier, M., Brawand, D., Zhang, X., Gu, H., Barthes, P., Kokkinaki, M., Nef, S., Gnirke, A., et al. (2013). Cellular source and mechanisms of high transcriptome complexity in the mammalian testis. *Cell Rep.* 3, 2179–2190.
- Tan, M., Luo, H., Lee, S., Jin, F., Yang, J.S., Montellier, E., Buchou, T., Cheng, Z., Rousseaux, S., Rajagopal, N., et al. (2011). Identification of 67 histone marks and histone lysine crotonylation as a new type of histone modification. *Cell* 146, 1016–1028.
- Trapnell, C., Williams, B.A., Pertea, G., Mortazavi, A., Kwan, G., van Baren, M.J., Salzberg, S.L., Wold, B.J., and Pachter, L. (2010). Transcript assembly and quantification by RNA-seq reveals unannotated transcripts and isoform switching during cell differentiation. *Nat. Biotechnol.* 28, 511–515.
- Vourekas, A., Zheng, Q., Alexiou, P., Maragkakis, M., Kirino, Y., Gregory, B.D., and Mourelatos, Z. (2012). Mili and Miwi target RNA repertoire reveals piRNA biogenesis and function of Miwi in spermiogenesis. *Nat. Struct. Mol. Biol.* 19, 773–781.
- Walker, M., Billings, T., Baker, C.L., Powers, N., Tian, H., Saxl, R.L., Choi, K., Hibbs, M.A., Carter, G.W., Handel, M.A., et al. (2015). Affinity-seq detects genome-wide PRDM9 binding sites and reveals the impact of prior chromatin modifications on mammalian recombination hotspot usage. *Epigenetics Chromatin* 8, 31.
- Wasik, K.A., Tam, O.H., Knott, S.R., Falcatori, I., Hammell, M., Vagin, V.V., and Hannon, G.J. (2015). RNF17 blocks promiscuous activity of PIWI proteins in mouse testes. *Genes Dev.* 29, 1403–1415.
- Watanabe, T., Cheng, E.C., Zhong, M., and Lin, H. (2015). Retrotransposons and pseudogenes regulate mRNAs and lncRNAs via the piRNA pathway in the germline. *Genome Res.* 25, 368–380.
- Weake, V.M., and Workman, J.L. (2008). Histone ubiquitination: triggering gene activity. *Mol. Cell* 29, 653–663.
- Yamamoto, Y., Watanabe, T., Hoki, Y., Shirane, K., Li, Y., Ichiiyanagi, K., Kuramochi-Miyagawa, S., Toyoda, A., Fujiyama, A., Oginuma, M., et al. (2013). Targeted gene silencing in mouse germ cells by insertion of a homologous DNA into a piRNA generating locus. *Genome Res.* 23, 292–299.
- Yu, Y., Gu, J., Jin, Y., Luo, Y., Preall, J.B., Ma, J., Czech, B., and Hannon, G.J. (2015). Panoramix enforces piRNA-dependent cotranscriptional silencing. *Science* 350, 339–342.
- Yue, F., Cheng, Y., Breschi, A., Vierstra, J., Wu, W., Ryba, T., Sandstrom, R., Ma, Z., Davis, C., Pope, B.D., et al. (2014). A comparative encyclopedia of DNA elements in the mouse genome. *Nature* 515, 355–364.
- Yuen, B.T., Bush, K.M., Barrilleaux, B.L., Cotterman, R., and Knoepfler, P.S. (2014). Histone H3.3 regulates dynamic chromatin states during spermatogenesis. *Development* 141, 3483–3494.
- Zhang, Y., Liu, T., Meyer, C.A., Eeckhoute, J., Johnson, D.S., Bernstein, B.E., Nusbaum, C., Myers, R.M., Brown, M., Li, W., et al. (2008). Model-based analysis of ChIP-seq (MACS). *Genome Biol.* 9, R137.

- Zhang, Y., Lin, Y.H., Johnson, T.D., Rozek, L.S., and Sartor, M.A. (2014a). PePr: a peak-calling prioritization pipeline to identify consistent or differential peaks from replicated ChIP-seq data. *Bioinformatics* *30*, 2568–2575.
- Zhang, Z., Wang, J., Schultz, N., Zhang, F., Parhad, S.S., Tu, S., Vreven, T., Zamore, P.D., Weng, Z., and Theurkauf, W.E. (2014b). The HP1 homolog rhino anchors a nuclear complex that suppresses piRNA precursor splicing. *Cell* *157*, 1353–1363.
- Zhou, H., Grubisic, I., Zheng, K., He, Y., Wang, P.J., Kaplan, T., and Tjian, R. (2013). Taf71 cooperates with Trf2 to regulate spermiogenesis. *Proc. Natl. Acad. Sci. USA* *110*, 16886–16891.

STAR★METHODS

KEY RESOURCES TABLE

REAGENT or RESOURCE	SOURCE	IDENTIFIER
Antibodies		
Mouse anti-HA	BioLegend	Cat# 901501; RRID: AB_2565006
Rabbit anti-Phospho-Histone H2A.X (Ser139)	Cell Signaling	Cat# 9718; RRID: AB_2118009
Mouse anti-Phospho-Histone H2A.X (Ser139)	Millipore	Cat# 05-636; RRID: AB_309864
Mouse anti-SYCP3	Santa Cruz	Cat# sc-74568; RRID: AB_2197355
Rabbit anti-SYCP3	Abcam	Cat# ab15093; RRID: AB_301639
Rabbit anti-SYCP1	Abcam	Cat# ab15090; RRID: AB_301636
Mouse anti-MLH1	BD Biosciences	Cat# 550838; RRID: AB_2297859
Rabbit anti-mCherry	Abcam	Cat# ab167453; RRID: AB_2571870
Mouse anti-Pol II	Abcam	Cat# ab817; RRID: AB_306327
Mouse anti-FLAG	Sigma-Aldrich	Cat# F3165; RRID: AB_259529
Rat anti-mCherry	ThermoFisher Scientific	Cat# M11217; RRID: AB_2536611
Rabbit anti-A-MYB	Sigma-Aldrich	Cat# HPA008791; RRID: AB_1078540
Rabbit anti-LINE1 ORF1p	Alex Bortvin lab	(Martin and Branciforte, 1993)
Chemicals, Peptides, and Recombinant Proteins		
SuperScript II Reverse Transcriptase	ThermoFisher Scientific	Cat# 18064022
DNA Pol I	ThermoFisher Scientific	Cat# EP0041
Tn5 Transposase enzyme	Illumina	Cat# FC-121-1031
Critical Commercial Assays		
Dynabeads mRNA Purification Kit	ThermoFisher Scientific	Cat# 61006
Nextera DNA Sample Preparation Kit	Illumina	Cat# FC-121-1031
NEBNext Ultra Directional RNA Library Prep Kit for Illumina	New England BioLabs	Cat# E7420S
NEBNext Multiplex Small RNA Library Prep Set for Illumina	New England BioLabs	Cat# E7330S
SimpleChIP Enzymatic Chromatin IP Kit	Cell Signaling	Cat# 9003
DNA SMART ChIP-Seq Kit	Clontech	Cat# 634865
Deposited Data		
Raw and analyzed data	This paper	GEO: GSE81470
Analyzed ChIP-seq data	Cistrome	http://cistrome.org
Experimental Models: Organisms/Strains		
Mouse: Btbd18 knockout	This paper	N/A
Mouse: Tg(FLAG-Btbd18-mCherry)	This paper	N/A
Oligonucleotides		
Primer: Btbd18 knockout mice, WT-Forward: CTTGAAATTACCAGCTCCC	This paper	N/A
Primer: Btbd18 knockout mice, WT-Reverse: GAACTCTAACCTGCCCTCC	This paper	N/A
Primer: Btbd18 knockout mice, KO-Forward: GAAGGTGCCACTCCCACTG	This paper	N/A
Primer: Btbd18 knockout mice, KO-Reverse: ACCAGCCAAACAATGAAA	This paper	N/A
Primer: Tg(FLAG-Btbd18-mCherry) mice, TG-Forward: CCGACTACTTGAAGCTGTCCTT	This paper	N/A

(Continued on next page)

Continued

REAGENT or RESOURCE	SOURCE	IDENTIFIER
Primer: Tg(FLAG-Btd18-mCherry) mice, TG-Reverse: CATGGTCTTCTTCTGCATTACG	This paper	N/A
Primers for RT-PCR, see Table S3	This paper	N/A
Software and Algorithms		
Bowtie	(Langmead et al., 2009)	http://bowtie-bio.sourceforge.net
TopHat v2.1	(Kim et al., 2013)	http://www.ccb.jhu.edu/software/tophat
DESeq2 v1.10.1	(Love et al., 2014)	https://bioconductor.org/packages/release/bioc/html/DESeq2.html
Cufflinks	(Trapnell et al., 2010)	https://github.com/cole-trapnell-lab/cufflinks
RepEnrich strategy	(Criscione et al., 2014)	N/A
R	N/A	https://www.r-project.org
GOrilla	(Eden et al., 2009)	http://cbl-gorilla.cs.technion.ac.il
DeepTools	(Ramirez et al., 2014)	http://deeptools.ie-freiburg.mpg.de/
Cistrome	(Mei et al., 2017)	http://cistrome.org/db
MACS2	(Zhang et al., 2008)	https://github.com/taoliu/MACS
PePr v 1.0.8	(Zhang et al., 2014a, 2014b)	https://github.com/shawnzhangyx/PePr

CONTACT FOR REAGENT AND RESOURCE SHARING

Further information and requests for reagents may be directed to, and will be fulfilled by, the Lead Contact, Jurrien Dean (jurrien.dean@nih.gov).

EXPERIMENTAL MODEL AND SUBJECT DETAILS

All animal studies were performed in accordance with guidelines of the Animal Care and Use Committee of the National Institutes of Health under a Division of Intramural Research, NIDDK approved animal study protocol. Unless otherwise noted, chemicals and other reagents were obtained from Sigma-Aldrich and restriction enzymes were obtained from New England Biolabs. Microscopic images were exported as full-resolution TIF files and processed in Photoshop CS6 (Adobe) by adjusting brightness and contrast.

METHOD DETAILS**Mice**

The *Btd18* gene was targeted in mouse embryonic stem (ES) cells by homologous recombination to remove exon 5. G418 resistant ES cell clones were selected by PCR with primers encompassing either the long (GCCACCGTTTCGCCACTAA, CCTACCCGCTTCATTGCT, 7 kb) or short (ATCGCATTGTCTGAGTAGGT, CACGGAAGAAAGCGTAAGG, 2 kb) arm and verified by Southern blot. Correctly targeted ES cells were injected into wildtype blastocysts to generate chimeric mice and heterozygotes were produced by germline transmission of the null allele. Primers for genotyping the *Btd18* knockout mice include *WT-Forward* and *WT-Reverse* with a 384 bp PCR product; *KO-Forward* and *KO-Reverse* with a 408 bp PCR product. Platinum Blue PCR SuperMix (ThermoFisher Scientific) was used for genotyping using the following conditions: 94°C for 2 min followed by 32 cycles of 94°C for 30 s, 58°C for 30 s, 72°C for 30 s, and a final extension step of 72°C for 5 min. To test fertility, pairs of WT and KO (homozygous *Btd18*^{Null}) female mice were co-caged with male mice to determine the number and size of litters.

To establish FLAG-*Btd18*-mCherry transgenic mice, *Btd18* cDNA with a FLAG tag added at the 5' end and a stop codon removed at 3' end was cloned from total RNA isolated from 4-cell mouse embryos. The resultant DNA fragment was inserted into the pmCherry-N1 vector (Clontech) with the promoter replaced by a 3.2 kb DNA sequence upstream of transcription start site of *Btd18*. The fidelity of the construct was confirmed by DNA sequence. To generate the transgenic mice, DNA fragment containing *Btd18* cDNA was injected into pronuclei of 1-cell zygotes for production of founders. Genotyping primers were *TG-Forward* and *TG-Reverse* that result in a 185 bp PCR product using the above conditions for PCR. p53 knockout mice were obtained from the Jackson Laboratory.

Histology Examination

Mouse testes were removed and fixed in Bouin's solution (Electron Microscopy Sciences) overnight at room temperature. Samples were washed with PBS, then 70% alcohol and stored at 4°C in 70% alcohol. Samples were embedded in paraffin, sectioned (5 μm)

and mounted on slides prior to staining with periodic acid-Schiff (PAS) and hematoxylin and eosin (H&E). An AxioPlan 2 microscope (Carl Zeiss) with an AxioCam ERc5s camera (Carl Zeiss) was used for imaging.

For TUNEL staining, testes were fixed (overnight, 4°C) in 4% paraformaldehyde, embedded in paraffin and sectioned (5 µm). TUNEL staining was performed using ApopTag Peroxidase In Situ Apoptosis Detection kit (EMD Millipore). To co-stain with γ H2A.X, the TUNEL Apo-Green Detection kit (BioTools) was used and DNA was stained with DAPI. Fluorescent images were obtained with a LSM 780 confocal/multiphoton microscope (Carl Zeiss) (100x/1.4, 63x/1.2W or 20x/0.8 objectives).

Preparation of Testicular Frozen Sections for Immunofluorescence

Testes were fixed in 4% paraformaldehyde for 16 hr at 4°C and washed with PBS. Samples were then sequentially soaked in 15% and 30% sucrose in PBS at 4°C for 16 hr and embedded in Tissue-Tek O.C.T. (Electron Microscopy Sciences) on dry ice and blocks were stored at -80°C. 10-15 µm thick cryosections were cut on a Leica CM3050 S Research Cryostat and stored at -20°C.

To perform immunofluorescence, frozen testicular sections were thrice washed with PBS and permeabilized (PBS, 0.5% Triton X-100, 20 min, room temperature). Slides were blocked (30 min, room temperature) with SuperBlock Blocking Buffer (Thermo Fisher Scientific) containing 0.05% Tween-20. Slides were then incubated with primary antibody (diluted 1:100, SuperBlock Blocking Buffer, 0.05% Tween-20, overnight, room temperature) followed by incubation (2 hr, room temperature) with an Alexa Fluor secondary antibody (ThermoFisher Scientific). DNA was stained with Hoechst and images were obtained with a LSM 780 confocal/multiphoton microscope.

Meiotic Chromosome Spreads for Immunofluorescence

Testes were collected, de-capsulated into 100 mM sucrose and chopped/pipetted to release germ cells. Cells were added to slides coated with 1% paraformaldehyde and dried (> 1 hr) in a humidified chamber. Slides were then washed with 0.4% Photo-Flo 200 Solution (Electron Microscopy Sciences), dried well and stored at -20°C.

For immunofluorescence, meiotic spreads were blocked (30 min, room temperature) and incubated with primary antibody (overnight, room temperature) followed by incubation (2 hr, room temperature) with Alexa Fluor secondary antibody. DAPI was used to stain DNA. An AxioPlan 2 microscope (Carl Zeiss) with an AxioCam MRm camera (Carl Zeiss) was used for imaging.

Realtime RT-PCR

RNeasy Mini Kit (Qiagen) was used to isolate total RNA. SuperScript III First-Strand Synthesis System (Thermo Fisher Scientific) was used for reverse transcription. iTaq Universal SYBR Green Supermix (Bio-Rad) was used for realtime PCR to assess transcript abundance of *Btbd18* and piRNA precursors relative to *Gapdh*.

Fluorescence-Activated Cell Sorting (FACS)

For isolation of testicular cells (Yuen et al., 2014; Chang et al., 2011), testes were collected and de-capsulated in Gey's balanced salt solution (GBSS) on ice. Tubules were transferred to 20 ml Digest Solution I, shaken (80 rpm, 35°C, 20 min) and precipitated by vertical standing (room temperature, 2-5 min). 500 µl of tubules at the bottom were transferred to Digest Solution II (10 ml for wildtype, 2 ml for KO). Tubules were shaken (80 rpm, 35°C, 20 min) and fetal bovine serum (FBS, ThermoFisher Scientific) was added to 15% final concentration. Cells were filtered through a pre-wetted 40 µm cell strainer (Corning). The cell concentration was adjusted to $1 \times 10^6 \text{ ml}^{-1}$ with 6 µg/ml Hoechst 33342 in Digest Solution III. Propidium iodide (PI) was added to 2 µg/ml just before cell sorting to exclude dead cells. Digest Solution I: GBSS, 200 µg/ml DNase I, 0.5 mg/ml collagenase IA. Digest Solution II: GBSS, 200 µg/ml DNase I, 1 mg/ml trypsin, 5 µg/ml Hoechst 33342. Digest Solution III: GBSS, 200 µg/ml DNase I, 15% FBS.

For FACS analysis, testicular cells were analyzed on a MoFlo Astrios EQ high speed cell sorter (Beckman Coulter) in a BSL2 enclosure. Flow data analysis was performed using Summit software V6.3.016900 (Beckman Coulter). The flow rate was adjusted to roughly 5,000 events/sec. PI fluorescence was captured using a 592 nm laser, with a 620/29 nm pass for detection. Hoechst 33342 fluorescence was captured using a UV (355 nm) laser, with a 448/59 nm pass for Hoechst blue detection and a 641/20 nm pass for Hoechst red detection. Different testicular cell populations were gated based on Hoechst Blue-Red profile as well as forward scatter properties. Cells were sorted into GBSS supplemented with 15% FBS and kept on ice. Freshly isolated cells were immediately used for ATAC-seq library preparation or lysed in TRI Reagent for RNA-seq library preparation.

RNA-Seq Library Preparation

Testes samples were washed in PBS after dissection and kept in RNAlater Stabilization Solution (ThermoFisher Scientific) at -20°C until use. Total RNA was isolated using TRI Reagent per instructions of the manufacturer. mRNA was purified by Dynabeads mRNA Purification Kit (ThermoFisher Scientific) followed by first strand cDNA synthesis with SuperScript II Reverse Transcriptase (ThermoFisher Scientific).

For second strand cDNA synthesis, the samples were incubated for 2 hr at 16°C in: 20 µL of first strand cDNA synthesis mix, 10 µL of 10x second strand buffer (500 mM Tris-HCl pH 7.5, 50 mM MgCl₂, 10 mM DTT), 3 µL of dNTP mix (10 mM), 1 µL of RNaseH (2U/µL), 5 µL of DNA Pol I (10U/µL) and water was added to 100 µL. The libraries were constructed with Nextera DNA Sample Preparation Kit (Illumina) per the manufacturer's protocol. RNA-seq libraries from sorted spermatocytes and round spermatids were prepared using NEBNext Ultra Directional RNA Library Prep Kit for Illumina (New England BioLabs) according to manufacturer's instructions.

Small RNA-Seq Library Preparation

To prepare small RNA-seq libraries (Roovers et al., 2015), total RNA was isolated from mouse testes using TRI Reagent. For periodate reaction and β -elimination, 13.5 μ l (20 μ g) total RNA was incubated (10 min, room temperature) with 4 μ l 5x borate buffer (148 mM borax, 148 mM boric acid, pH 8.6, ThermoFisher Scientific) as well as 2.5 μ l freshly dissolved 200 mM NaIO₄ (ThermoFisher Scientific). Glycerol (2 μ l, ThermoFisher Scientific) was added to quench unreacted NaIO₄ and incubated for an additional 10 min at room temperature. 380 μ l 1x borate buffer was added and RNA was precipitated with ethanol (1 hr, -80°C). RNA was dissolved in 50 μ l 1x borax buffer (30 mM borax and 30mM boric acid, 17.5 mM NaOH, pH 9.5) and incubated (90 min, 45°C) prior to addition of 450 μ l 1x borate buffer and 20 μ g of glycogen. RNA was precipitated with ethanol (1 hr, -80°C), collected by centrifugation and dissolved in water. Periodate-reacted RNAs were shortened during β -elimination by 1 nt at the 3' end with monophosphates and were unable to be amplified during library preparation. piRNAs were protected from β -elimination by 2'-O-methylation at 3' end and therefore were enriched in small RNA-seq libraries. NEBNext Multiplex Small RNA Library Prep Set for Illumina (New England BioLabs) was used for small RNA-seq library construction per the manufacturer's instructions. Generally, 1 μ g total RNA was subjected to 3' and 5' adapter ligation, reverse transcribed, PCR amplified, followed by size selection with AMPure XP beads (Beckman Coulter) for deep sequencing.

ChIP-Seq Library Preparation

Testicular cells from 3-to-4-week-old males were prepared as in the section on FACS. SimpleChIP Enzymatic Chromatin IP Kit (Cell Signaling) was used to perform ChIP assay from testicular cells. Generally, testicular cells (1×10^6 ml⁻¹) were crosslinked with 1% formaldehyde for 10 min at room temperature, and chromatin was digested with micrococcal nuclease into 150-900 bp DNA/protein fragments and immunoprecipitated with Protein G magnetic beads. After reversal of protein-DNA cross-links, DNA was purified with spin columns. For ChIP-seq analysis, 8-12 male mice ($\sim 5 \times 10^7$ testicular cells) were used for precipitation of chromatin complexes containing BTBD18 and 2-8 male mice ($\sim 5 \times 10^6$ testicular cells) were used for precipitation of chromatin complexes containing A-MYB or RNA Pol II. Libraries were further generated using DNA SMART ChIP-Seq Kit (Clontech) per the manufacturer's instructions.

ATAC-Seq Library Preparation

ATAC-seq libraries were constructed (Buenrostro et al., 2015; Buenrostro et al., 2013) using 5×10^4 spermatocytes freshly isolated from individual mice. Cells were centrifuged (500 x g, 5 min, 4°C), washed with 100 μ l PBS and re-suspended in 50 μ l of lysis buffer (10 mM Tris pH 7.5, 10 mM NaCl, 3 mM MgCl₂, 0.1% IGEPAL). After centrifugation (500 x g, 10 min, 4°C), pelleted nuclei were re-suspended in 50 μ l of transposition reaction consisting of 2x Tagmentation buffer (20 μ l), water (18 μ l) and Tn5 Transposase enzyme (2 μ l, Illumina). After incubation (30 min, 37°C) with gentle mixing, DNA was purified using a MinElute PCR Purification Kit (Qiagen) and eluted into 20 μ l of elution buffer.

Transposed DNA was amplified using barcoded PCR primers. PCR cycling conditions were 72°C for 5 min and 98°C for 30 s followed by 10 cycles of 98°C for 10 s, 63°C for 30 s, 72°C for 1 min. DNA fragments of nucleosome free regions (between primer-dimers and mononucleosome bands) corresponding to sequence insert < 100 bp were excised from 1.4% agarose gel and purified using MinElute Gel Extraction Kit (Qiagen). Libraries were eluted with 10 μ l elution buffer for analysis of size distribution.

Common Library Analyses

All libraries were analyzed by Agilent 2100 Bioanalyzer system with the High Sensitivity DNA Kit for proper quantity and size distribution. PicoGreen was used for DNA quantification before sequencing on Illumina HiSeq 2500 as single-end 50-bp reads.

QUANTIFICATION AND STATISTICAL ANALYSIS

RNA-Seq Data Analysis

Raw reads were processed with cutadapt v1.8.1 (<https://cutadapt.readthedocs.io>) to remove adapters and perform quality trimming with default parameters except for: quality-cutoff =20, minimum-length =25, and overlap =10. Trimmed reads were mapped to the UCSC mm10 assembly using TopHat v2.1 (<http://ccb.jhu.edu/software/tophat>) with default parameters. Reads were annotated based on genomic locations of mm10 genes and 214 piRNA precursors. Reads were counted in exons of the UCSC for mm10, using featureCounts (<http://subread.sourceforge.net>) from the Subread package V1.4.6-p3. Differential expression of genes for all pairwise comparisons was assessed by DESeq2 v1.10.1 (<https://bioconductor.org/packages/release/bioc/html/DESeq2.html>) with internal normalization of reads to correct for library size and RNA composition bias. Differentially regulated genes in the DESeq2 analysis were defined as those which were more than two-fold increased or decreased with adjusted P < 0.05. Normalized bigWig coverage tracks were generated by size factors estimated by DESeq2. Cufflinks (<https://github.com/cole-trapnell-lab/cufflinks>) was used to calculate FPKM value. Dot-and-box plot was generated by R. Principal component analysis (PCA) was performed using log2 (FPKM+0.01) of all genes or piRNA precursors by R. Gene ontology (GO) analysis was performed using GOrilla (<http://cbl-gorilla.cs.technion.ac.il/>).

RepEnrich strategy (Criscione et al., 2014) was used to analyze transposable elements. Generally, Bowtie (<http://bowtie-bio.sourceforge.net/>) was used for mapping with the requirement that reads map uniquely using the -m 1 option. Reads mapping to multiple locations of the genome were remapped to a pseudogenome assemblies generated for each distinct repetitive element

subfamily. Sequences of transposable elements were downloaded from RepeatMasker (<http://www.repeatmasker.org/>). Bedtools (<https://bedtools.readthedocs.io/>) was used to count and summarize the uniquely-mapping reads that fall within an annotated repetitive element. Differential expression analysis was performed using the DESeq2.

Small RNA-Seq Data Analysis

After removing adaptors, rRNA and tRNA sequences were filtered before analysis. Remaining reads with sizes from 26 to 31 nt were mapped to the UCSC mm10 assembly using TopHat and only uniquely mapped reads were used for further analysis. piRNA abundance was obtained through normalization to miRNA counts (miRBase). To create averaged graphs for size distribution of small RNA-seq data, reads from biological replicates were summed up and normalized with total uniquely mapped reads.

ChIP-Seq and ATAC-Seq Data Analysis

Raw reads were processed with cutadapt v1.8.1 to remove adapters and perform quality trimming. Trimmed reads were mapped to the UCSC mm10 assembly using Bowtie with default parameters and only uniquely aligned sequences were retained. DeepTools (<http://deeptools.ie-freiburg.mpg.de/>) was used for normalization to generate read density plot from BAM or bigwig (analyzed by Cistrome from reported ChIP-seq results; <http://cistrome.org/db/>) files. Reported ChIP-seq results include TAF7L (GSM1229970), RFX2 (GSM1666996), H3K4me3 (GSM1202706), H3K9me3 (GSM1659047), H3K27me3 (GSM1202709), H3K36me3 (GSM1000067), pan-lysine-acetylation (GSM810674), H3K27ac (GSM1202714), H4K16ac (GSM1713739), H4K8ac (GSM1713736), pan-lysine-crotonylation (GSM810675). For BTBD18 occupancy (GSM2152920 and GSM2393968), peak calling was performed by MACS2 (<https://github.com/taoliu/MACS>) and PePr v 1.0.8 (<https://github.com/shawnzhangyx/PePr>), with input (GSM2152913 and GSM2393967) used as the control. MACS2 is more sensitive to detect peaks whereas PePr has very low scaling False Discovery Rate (FDR) (Zhang et al., 2014a, 2014b). For MACS2, default parameters with broad peak option and a broad-cutoff of 0.01 (q value) were used; for PePr, default parameters and a threshold of 0.001 (P value) were used with broad as peak type. For A-MYB occupancy, peak calling was performed with the same parameters, using input as the control.

Statistical Analysis

The two-tailed Student's t-test and the Wilcoxon rank sum test with continuity correction were used to calculate P values. Statistically significant values for $P < 0.05$, $P < 0.01$ and $P < 0.001$ are indicated by single, double and triple asterisk, respectively.

DATA AND SOFTWARE AVAILABILITY

The accession number for the sequencing data reported in this paper is GEO: GSE81470. The ChIP-seq data for Figure S6 is in Cistrome database.

Developmental Cell, Volume 40

Supplemental Information

**BTBD18 Regulates a Subset of piRNA-Generating
Loci through Transcription Elongation in Mice**

Liquan Zhou, Bertram Canagarajah, Yangu Zhao, Boris Baibakov, Keizo Tokuhiro, Dragan Maric, and Jurrien Dean

SUPPLEMENTAL FIGURES

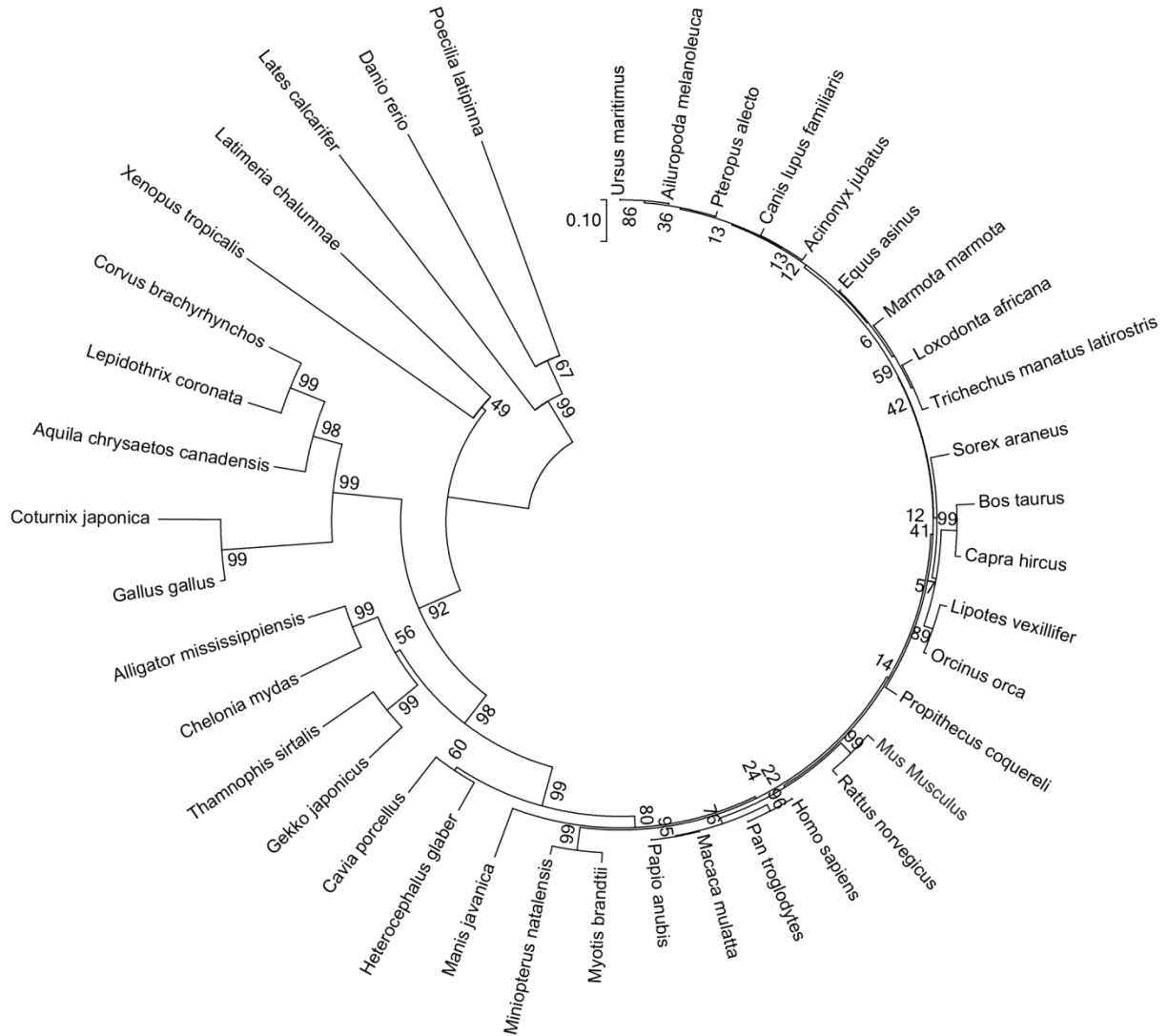


Figure S1. Evolutionary analyses of *Btbd18*. Related to Figure 1.

BTBD18 protein sequences from 40 species were used to generate an evolutionary tree in MEGA7. The evolutionary history was inferred using the Neighbor-Joining method. The percentages of replicate trees in which the associated taxa clustered together in the bootstrap test (500 replicates) are shown next to the branches. The tree is drawn to scale, with branch lengths in the same units as those of the evolutionary distances. The evolutionary distances were computed using the Poisson correction method and are in the units of the number of amino acid substitutions per site.

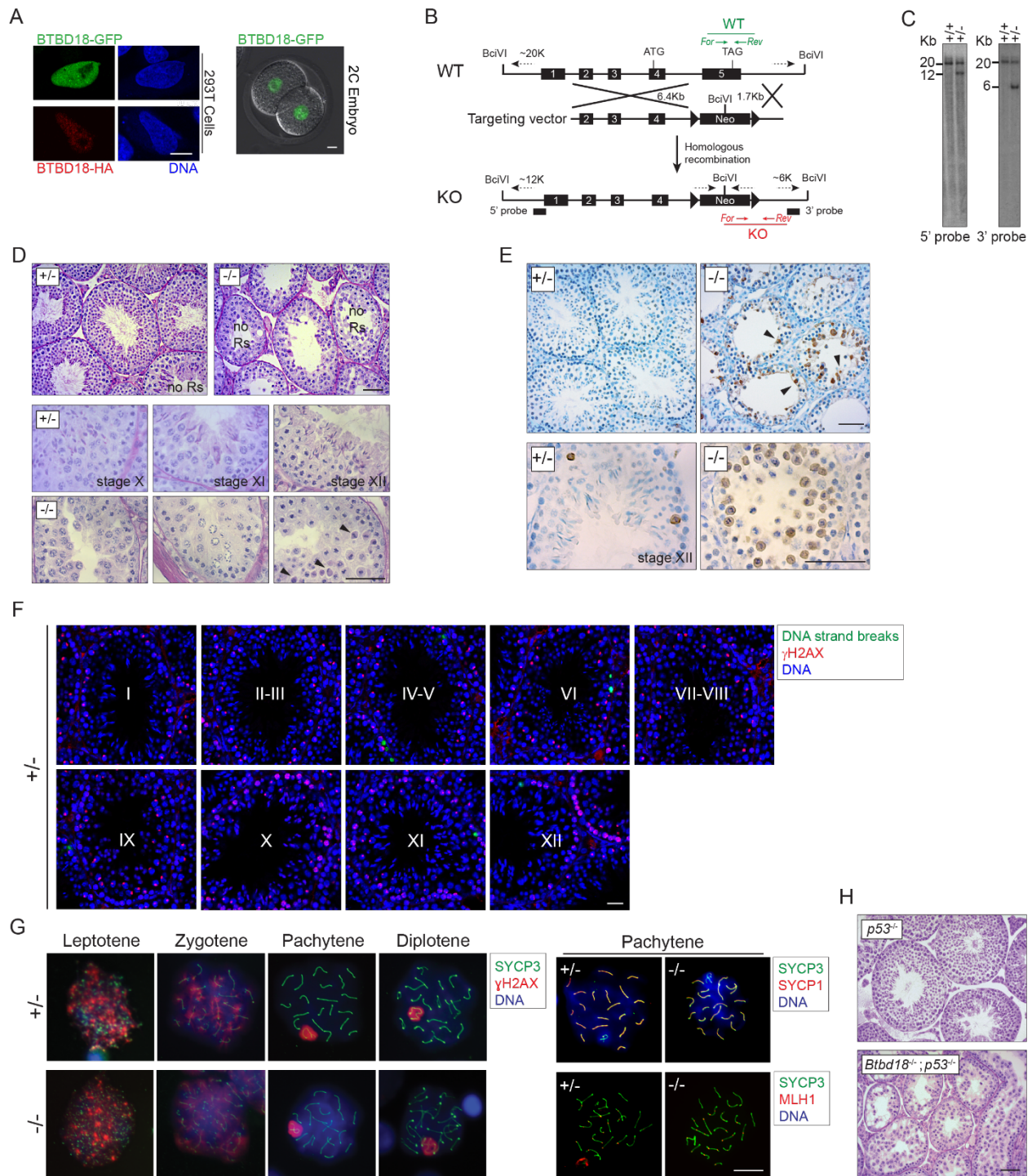


Figure S2. Generation of *Btd18* knockout mice. Related to Figure 1.

(A) Plasmids expressing BTBD18-GFP (top left panel) or BTBD18-HA (bottom left panel) were separately transfected into 293T cells for 24 hr followed by examination of protein localization by confocal microscope. BTBD18-GFP was detected by fluorescence and BTBD18-HA was stained with anti-HA antibody. cRNA (200ng/ μ l) encoding BTBD18-GFP was injected into 1-cell zygote and imaged at the 2-cell stage (right panel). Scale bar, 10 μ m.

(B) Schematic representation of targeting vector used in mouse embryonic stem (ES) cells to generate a *Btbd18*^{Null} allele. The location of the cassette and position of probes for Southern blot and primers for genotyping are shown. BciVI, restriction enzyme. ATG, start codon; TAG, stop codon; Neo, neomycin resistant cassette.

(C) Southern blotting of targeted ES cells using a 5' probe (left panel) and 3' probe (right panel) with sequences outside of the targeting vector (see B). Genotype: +/-, heterozygous; -/-, homozygous.

(D) Light microscopic images of testicular sections from 4-month-old control (heterozygous, +/-) and *Btbd18*^{Null} (homozygous, -/-) mice after staining with PAS/H&E. Top two panels (low magnification), tubules without round spermatids (Rs). Bottom six panels (high magnification to identify stage and cell type), tubules at stages X, XI and XII. Arrowheads, apoptotic cells. Scale bars, 50 μ m.

(E) TUNEL analysis of DNA strand breaks in paraffin embedded sections of testes from 8-week-old control (heterozygous, +/-) and *Btbd18*^{Null} (homozygous, -/-) mice. Top panels, low magnification. Arrowheads, apoptotic cells. Bottom panels of stage XII tubules (high magnification). Scale bars, 50 μ m.

(F) Fluorescent TUNEL staining of sections from 8-week-old control (heterozygous) testes. TdT labeling was used to indicate DNA strand breaks. Scale bar, 20 μ m.

(G) Meiotic chromosome spreads of spermatocytes from control (heterozygous) and *Btbd18*^{Null} (homozygous) testes document all meiotic phases (left panel), normal meiotic synapsis (top right panel) and recombination (bottom right panel) by immunolabelling key meiotic factors including SYCP3, SYCP1, γ H2A.X and MLH1. Scale bar, 10 μ m.

(H) Morphology of *p53*^{Null} (top panel) and *Btbd18*^{Null}; *p53*^{Null} (bottom panel) testes (20 \times /0.8 objectives). Note that the *p53* background does not rescue spermatogenesis in absence of BTBD18. Scale bar, 50 μ m.

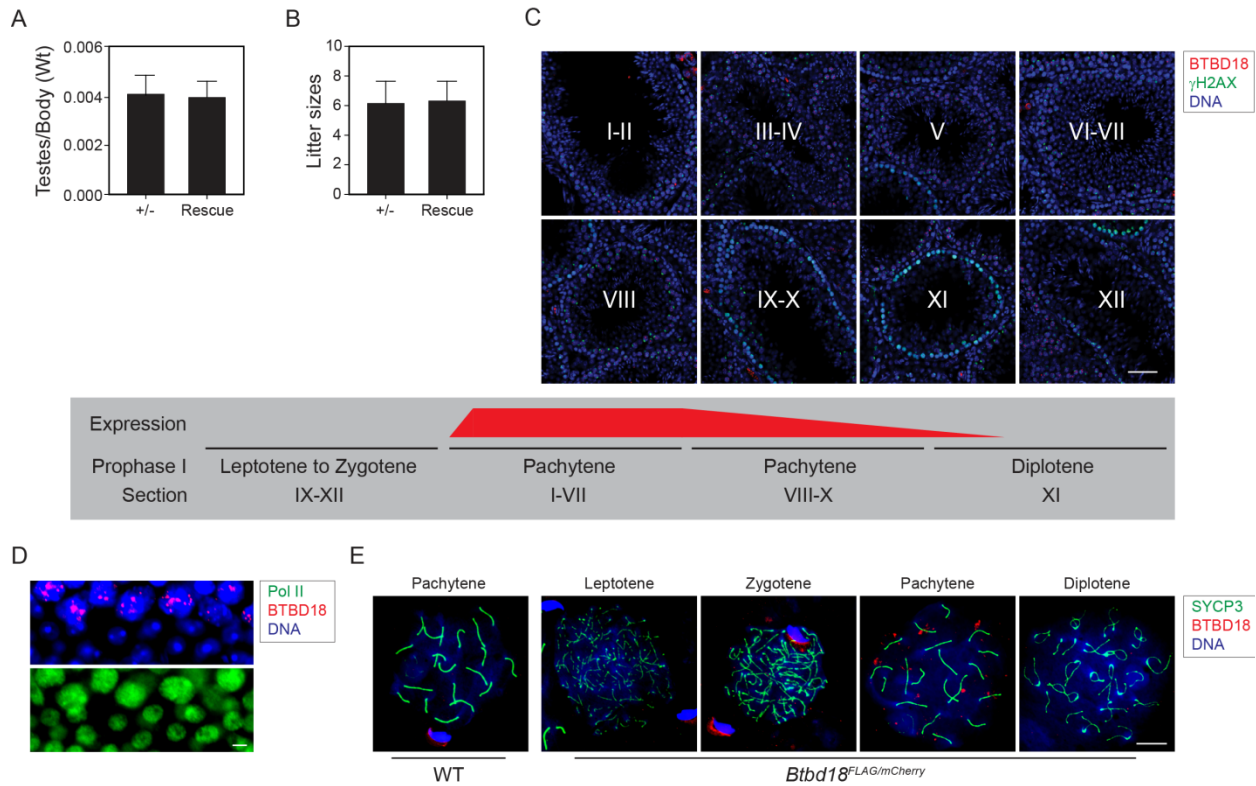


Figure S3. Localization of BTBD18^{FLAG/mCherry} protein in testes. Related to Figure 2.

(A) Three biological replicates of 8-week-old control (+/-, heterozygous) and *Btbd18* rescue (*Btbd18*^{Null}; *Btbd18*^{FLAG/mCherry}) males were used to determine the average ratio of testes to body weight ± SD.

(B) Fertility was determined with 10 litters from 3-to-9-month-old male mice of each genotype after crossing with wildtype females. Mean litter sizes ± SD.

(C) BTBD18^{FLAG/mCherry} expression in cross-sections of mouse seminiferous tubules from 8-week-old *Btbd18* rescue (*Btbd18*^{Null}; *Btbd18*^{FLAG/mCherry}) males after immunostaining antibodies to mCherry and γH2A.X. Scale bar, 50 μm. Roman numbers I-XII indicate spermatogenic stages.

(D) Nuclear localization of BTBD18^{FLAG/mCherry} and RNA Pol II in frozen testicular sections from *Btbd18*^{FLAG/mCherry} mice. Scale bar, 5 μm.

(E) Meiotic chromosome spreads of spermatocytes from wildtype (left) and *Btbd18*^{FLAG/mCherry} (right) mice were used to localize BTBD18^{FLAG/mCherry} in meiotic cells. Scale bar, 5 μm.

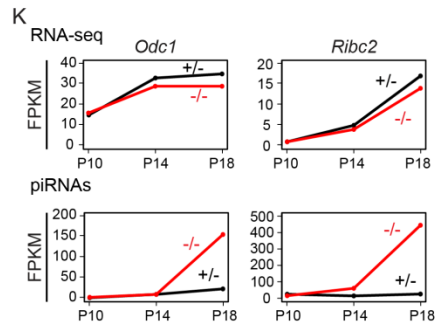
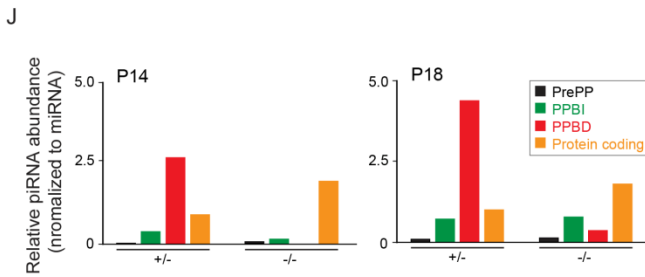
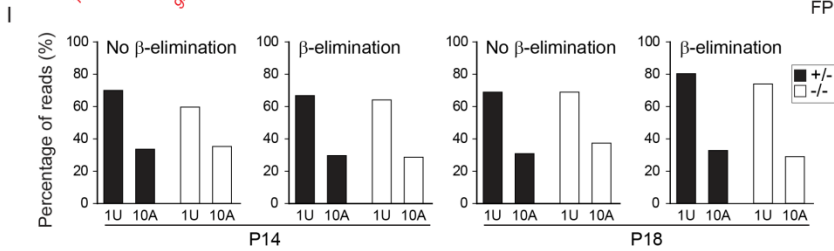
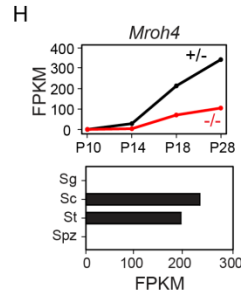
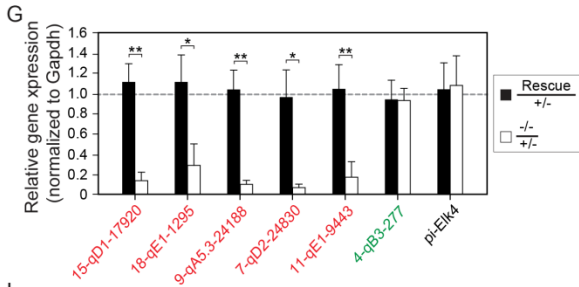
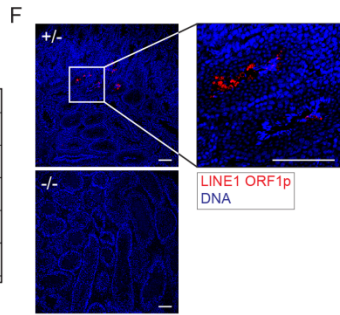
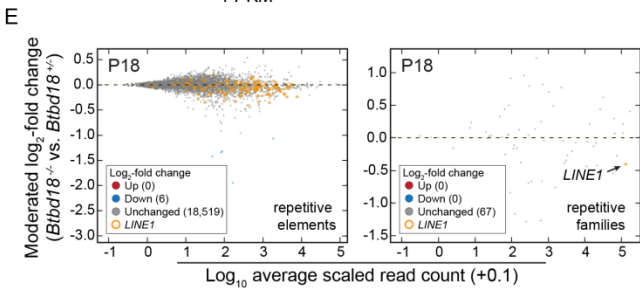
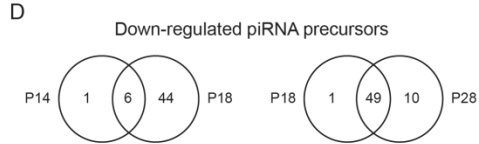
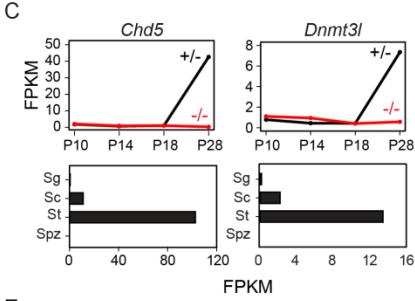
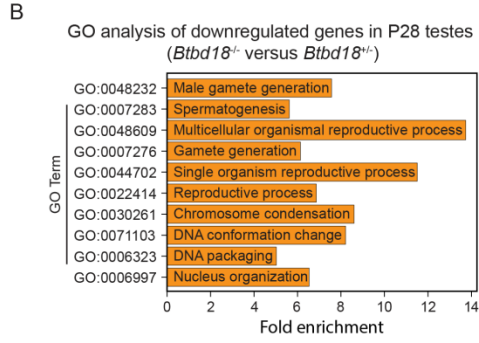
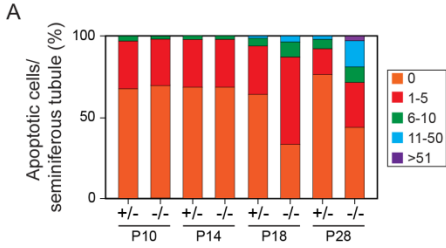


Figure S4. Transcriptome analysis of testes. Related to Figure 3-5.

(A) Quantification of TUNEL analysis of apoptotic cells in seminiferous tubule in control (+/-) and *Btbd18*^{Null} (-/-) testes from P10-P28.

(B) Gene ontology (GO) analysis of down-regulated genes in *Btbd18*^{Null} (-/-) testes at P28. Top 10 enriched GO terms are shown.

(C) Examples of genes (*Chd5*, *Dnmt3l*) which are significantly downregulated in *Btbd18*^{Null} testes at P28 (upper panels) and are enriched in wildtype spermatids (lower panels). Graphs represent an average of 2-3 biological replicates. Spermatogonia (Sg); spermatocytes (Sc); spermatids (St); spermatozoa (Spz).

(D) Venn diagrams documents overlap of downregulated genes examined at two developmental transitions, P14-P18 (left) and P18-P28 (right).

(E) RNA-seq analysis of repetitive elements which are not significantly changed in *Btbd18*^{Null} P18 testes. Each point represents one repetitive element (left panel) or a repetitive family (right panel). *LINE1* elements are circled in yellow.

(F) Immunofluorescence of LINE1 ORF1p in frozen testicular sections from 3-month old males shows that *LINE1* elements are not de-repressed in the absence (-/-) of BTBD18 protein. Scale bar, 100 μ m.

(G) The relative abundance of BD-PP (red), BI-PP (green) or prePP (black) piRNA precursor transcripts (mean of 3 biological replicates) in testes from 8-week-old *Btbd18* rescue (*Btbd18*^{Null}; *Btbd18*^{FLAG/mCherry}) and *Btbd18*^{Null} (-/-, homozygous) males were compared to the abundance in control (+/-, heterozygous) males, using *Gapdh* transcript as an internal control. Error bar, SD. * P <0.05; ** P <0.01 by two-tailed Student's t-test.

(H) *Mroh4*, enriched in spermatocytes and spermatids (lower panel) is significantly downregulated in *Btbd18*^{Null} testes (upper panel). Graphs represent an average of 2-3 biological replicates.

(I) Percentage of piRNA with U at the first position (1U) or A at position 10 (10A) for testes samples with indicated genotypes, treatment and age.

(J) Abundance of piRNAs derived from PrePP, PPBI, PPBD and protein-coding genes in testes samples with indicated genotypes and age. piRNA abundance was calculated from the number of reads obtained normalized to miRNA counts (miRBase).

(K) Transcript abundance (log₂ FPKM) and piRNA production (log₂ FPKM) of two representative protein coding genes in indicated genotypes and age. piRNA expression levels were normalized to total miRNA reads.

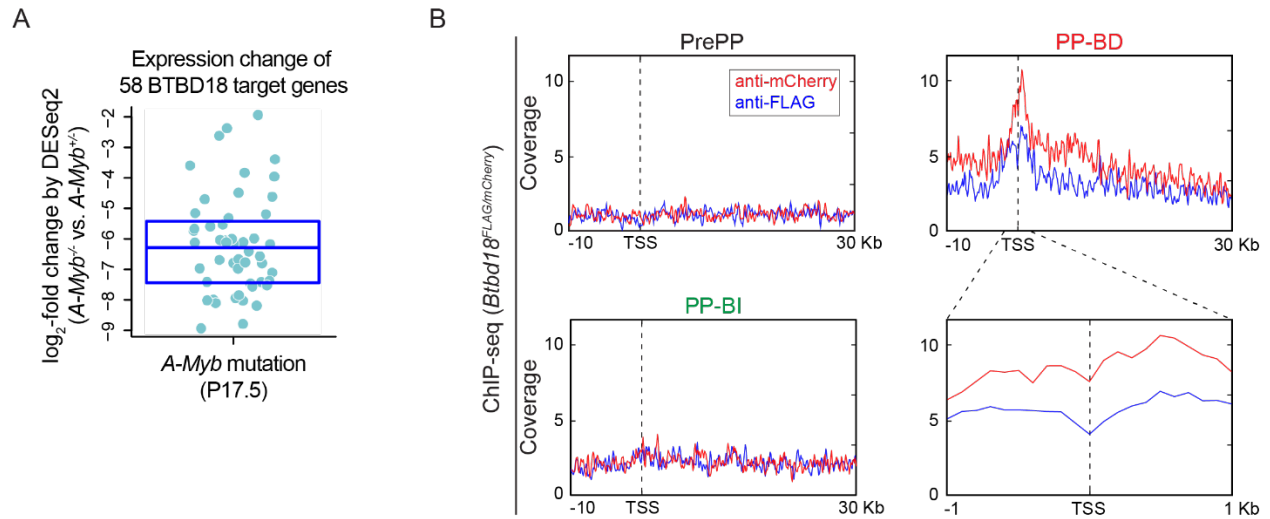


Figure S5. ChIP-seq analysis of BTBD18 in testes. Related to Figure 6.

(A) DESeq2 analysis for differential gene expression of 58 BTBD18 targets in *A-Myb* mutant testis at P17.5 (GSE44690).

(B) Read density profiles (deepTools normalized coverage) of ChIP-seq for PrePP, PP-BI and PP-BD populations with antibodies to FLAG (blue) or mCherry (red) in 100-bp bins. TSS, transcription start site.

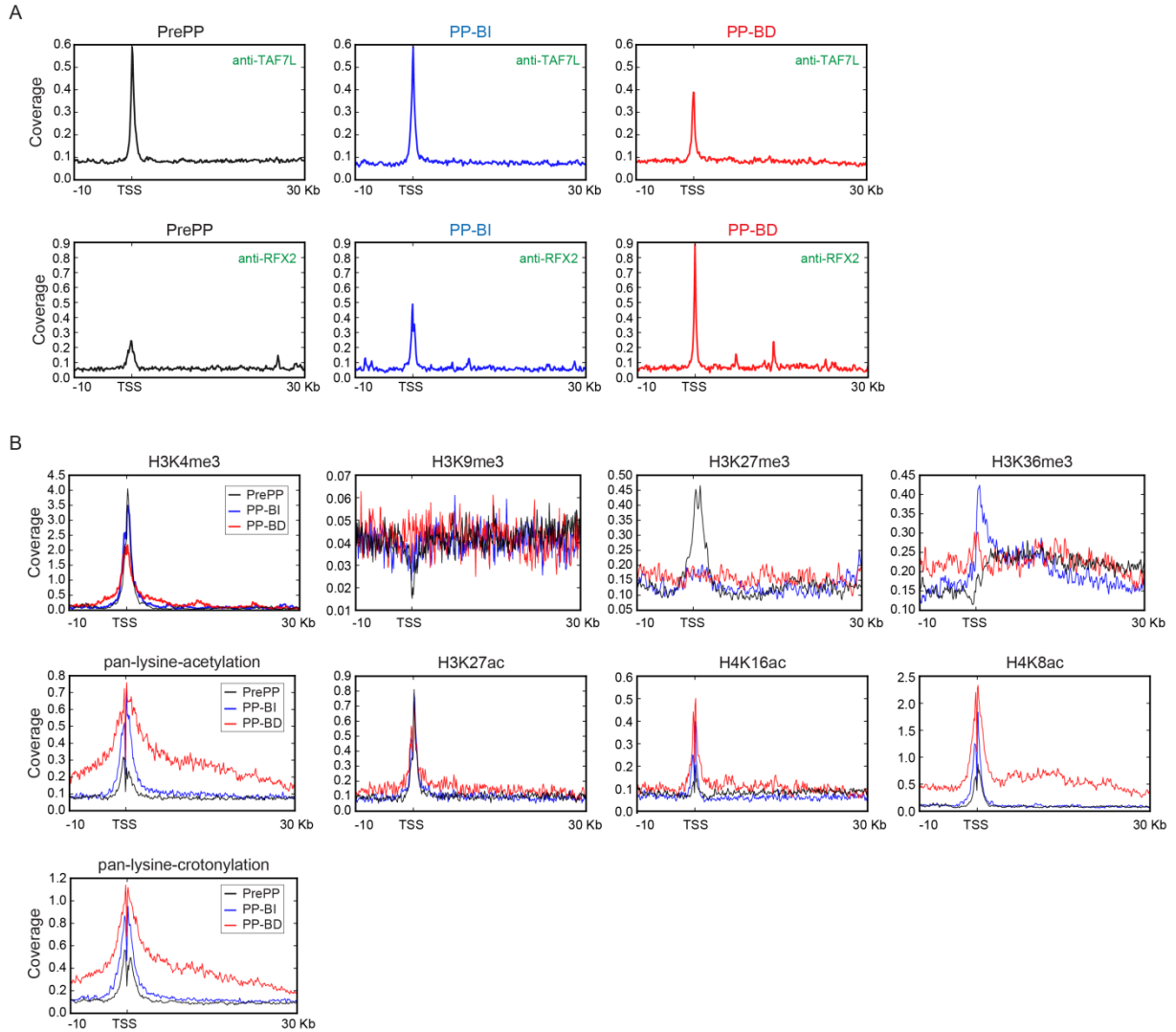


Figure S6. Chromatin structure analysis of piRNA precursors. Related to Figure 7. Read density profiles (deepTools normalized coverage) of reported ChIP-seq data (bigWig files generated by cistrome) for PrePP, PP-BI and PP-BD populations with antibodies to transcription factors (A) and histone modifications (B) in 100-bp bins.

SUPPLEMENTAL TABLES

Table S1. Genomic Locations of PrePP, PPBI and PPBD genes. Related to Figure 4.
See attached Excel table.

Table. S2. CHIP-seq Peaks of BTBD18. Related to Figure 6.
See attached Excel table.

Table S3. Primers for RT-PCR, related to STAR methods.

Primer name	Sequence	PCR product size (bp)
<i>Gapdh-For</i>	GGTTGTCTCCTGCGACTTCA	186
<i>Gapdh-Rev</i>	GGGTGGTCCAGGGTTTCTTA	
<i>Btbd18 -For</i>	CCCAACTCAGGTCATAAGG	339
<i>Btbd18 -Rev</i>	CAGAAGTGGTCGTGGAAGT	
<i>pi-Elk4-For</i>	CTGTCACCCAACCTGGCTAT	209
<i>pi-Elk4-Rev</i>	GAACACCAAGCCTCTCTTGC	
<i>4-qB3-277-For</i>	TCTTAGGCAATGGGGTTGTC	191
<i>4-qB3-277-Rev</i>	AGTGGGAAAATGAGCACCAC	
<i>15-qD1-17920-For</i>	AGCAACTATCTCCCGAGCAA	221
<i>15-qD1-17920-Rev</i>	GGCTTCCAGAAACAGAGCAC	
<i>18-qE1-1295-For</i>	AGCAGAGGCTATCTGGGTGA	219
<i>18-qE1-1295-Rev</i>	TTGACTCCTCAGCCTCCTGT	
<i>9-qA5.3-24188-For</i>	GCTCCAACCGTCTGTGGTAT	218
<i>9-qA5.3-24188-Rev</i>	AGACAGTGGTGTTCCCAAGG	
<i>7-qD2-24830-For</i>	CCACTTGGGGACACTGAACT	239
<i>7-qD2-24830-Rev</i>	CAGAGTCACCAGCTCCATCA	
<i>11-qE1-9443-For</i>	CAGAAAGAGCAGCCGTAACC	195
<i>11-qE1-9443-Rev</i>	ACCTGGGAGGTTTCATGTGAG	